

**A GUIDE FOR INTERPRETING  
DOPPLER VELOCITY PATTERNS:  
Northern Hemisphere Edition**

Rodger A. Brown and Vincent T. Wood  
NOAA/National Severe Storms Laboratory  
Norman, Oklahoma



Second Edition

June 2007



## PREFACE

Doppler weather radars provide valuable measurements that aid forecasters in preparing more accurate and timely warnings and short-term forecasts and that help other users to better understand a variety of atmospheric processes. Though computer algorithms are available to objectively interpret Doppler velocity data, weather decision makers also subjectively interpret the patterns found in Doppler velocity displays. This Guide was prepared to help Doppler radar users in the Northern Hemisphere become proficient in pattern interpretation—through the use of simulated patterns representing flow fields within clear air and widespread precipitation as well as within tropical cyclones and convective storms. The first edition of the Guide, prepared by the authors in 1987 under an agreement with the NEXRAD Joint System Program Office (forerunner of the WSR-88D Radar Operations Center), was used as part of initial WSR-88D training for National Weather Service forecasters. This second edition is slightly revised and contains Doppler velocity displays that use color scales that are color blind friendly. Since this Guide was prepared by federal government employees, it is not copyrighted. It may be freely copied and distributed with appropriate acknowledgments. PDF and HTML versions of the Guide, as well as the ability to download individual figures, are available at <http://publications.nssl.noaa.gov>.



## TABLE OF CONTENTS

	<u>Page</u>
1. BACKGROUND INFORMATION	1
1.1 Introduction	1
1.2 Review of Doppler Radar Principles	2
1.3 Organization of This Guide	5
2. INTERPRETATION OF DOPPLER VELOCITY PATTERNS IN CLEAR AIR AND WIDESPREAD PRECIPITATION	7
2.1 Introduction	7
2.2 Patterns Associated with Vertical Profiles having Constant Wind Direction	9
2.3 Patterns Associated with Nonuniform Horizontal Wind Fields	12
2.4 Patterns Associated with Vertical Profiles having Constant Wind Speed	14
2.5 Patterns Associated with Vertical Profiles of Varying Wind Speed and Direction	16
2.6 Patterns Associated with Vertical Discontinuities in the Wind Field	18
2.7 Patterns Associated with Horizontal Discontinuities in the Wind Field	20
3. INTERPRETATION OF DOPPLER VELOCITY PATTERNS WITHIN TROPICAL CYCLONES	22
4. INTERPRETATION OF DOPPLER VELOCITY PATTERNS WITHIN CONVECTIVE STORMS	26
4.1 Introduction	26
4.2 Patterns Associated with Constant Wind Speed and Direction	26
4.3 Patterns Associated with Axisymmetric Vortices	28
4.4 Patterns Associated with Axisymmetric Radial Flow	30
4.5 Mesocyclone and Divergence Patterns Viewed from Four Different Directions	32
4.6 Distortion of Doppler Velocity Patterns Owing to Proximity to the Radar	35
4.7 Patterns Associated with a Convergent/Divergent Mesocyclone	38
4.8 Patterns Associated with Two Mesocyclones having the Same Size and Strength	42
4.9 Patterns Associated with a Tornadic Vortex Signature within the Parent Mesocyclone	44
4.10 Patterns Associated with Two Divergence Regions	46
4.11 Patterns Associated with Flow Fields beneath Supercell Thunderstorms	48
4.12 Patterns Associated with Midaltitude Flow around a Thunderstorm Updraft Region	50
5. THE CHALLENGE	53
6. ACKNOWLEDGMENTS	54
REFERENCES	55



# 1. BACKGROUND INFORMATION

## 1.1 Introduction

Doppler radars have been used to study weather phenomena throughout the world since the mid 1950s (e.g., Rogers 1990). Initially, Doppler radars were used by the weather research and engineering communities to study phenomena ranging from clear air to severe thunderstorms. As the advantages of Doppler radars over conventional weather radar became known, interest developed in using Doppler radars for real-time operational applications. By the mid-1990s, Weather Surveillance Radar–1988 Dopplers (WSR–88Ds) and Terminal Doppler Weather Radars (TDWRs) were in operational use in the United States. WSR–88Ds are used for overall weather surveillance and warnings by the National Weather Service, U. S. Air Force, and Federal Aviation Administration (FAA). TDWRs are used by the FAA at selected airports to monitor wind conditions that would adversely affect aircraft take-offs and landings.

A Doppler radar typically measures three *base data* parameters: radar reflectivity factor (function of scatterer intensity), mean Doppler velocity within the radar sampling volume (function of the mean component of scatterer motion in the radial direction from the radar) and spectrum width (function of the variability of Doppler velocity values due to turbulence within and velocity shear across the sampling volume). Interpretations of reflectivity and Doppler velocity data acquired from quasi-horizontal radar scans are based primarily on the identification of recognizable reflectivity and Doppler velocity patterns or “signatures.”

Computer algorithms are routinely used with WSR–88Ds for automatically processing the data and identifying significant Doppler velocity and reflectivity features. These *derived* products are available to the radar user shortly after the data are collected. Algorithms developed for WSR–88Ds are discussed in Federal Meteorological Handbook 11, Part C (OFC 2006) as well as in other publications, such as the papers that appeared in the June 1998 issue of *Weather and Forecasting*. Even with the availability of algorithm output, forecast and warning decisions frequently require user interpretation of Doppler velocity signatures on radar displays.

The goal of this Guide is to acquaint prospective users with the interpretation of Doppler velocity signatures. Through the use of simulated Doppler velocity displays, the reader is introduced to a number of patterns associated with basic subsynoptic-scale, mesoscale, and storm-scale flow patterns.

## 1.2 Review of Doppler Radar Principles

### a. Concept of Range Folding

A pulse Doppler radar, like a conventional weather radar, transmits a series of pulses that are separated by a distance,  $d$ , in the radial direction from the radar (e.g., Battan 1973; Rinehart 2004). The separation distance is a function of the rate at which pulses are transmitted ( $PRF$ , pulse repetition frequency) and the speed,  $c$ , at which radar energy propagates through the atmosphere

$$d = c/PRF, \quad (1.2.1)$$

where  $c$  is  $3 \times 10^8 \text{ m s}^{-1}$  ( $5.8 \times 10^8 \text{ kt}$ ). Some of the transmitted energy is reradiated back to the radar by scattering regions (precipitation, insects, refractivity gradients, etc.). The maximum range to which a pulse can travel and return before the next pulse is transmitted is one-half the separation distance,  $d$ . This maximum range is defined as

$$r_{max} = c/(2 PRF). \quad (1.2.2)$$

The range of a scattering region from the radar is computed from the time that the pulse is transmitted until signal is received back at the radar. The tacit assumption is that the returned signal is from the pulse that was just transmitted. If the scattering region is at a range greater than  $r_{max}$ , return from that region will not be received by the radar until after the next pulse is

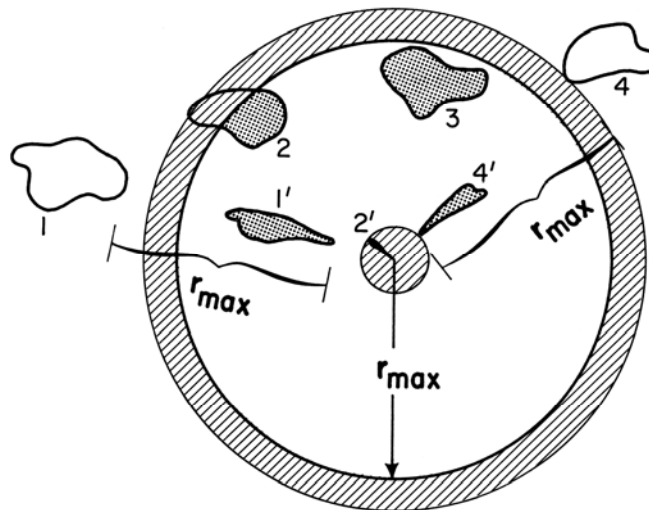


**Fig. 1.2.1.** Examples of range folding for a line of four storms oriented from the WSW to the ENE. The circle at distance  $r_{max}$  from the radar is the end of the first trip. Shaded areas represent the locations of measured radar return (radar “echoes”); those labeled with primed numbers were received from storms located beyond the first trip. Hatched area at center represents radar return from ground targets. If the second trip were displayed, all echoes in the first trip would be repeated in the second trip (echoes corresponding to the shaded portions of storms 2 and 3 would appear as wider echoes beyond the top of the figure); the ground return around the radar would appear as the shaded ring at the beginning of the second trip.

transmitted. Such return is referred to as “second-trip” return because the actual range of the scattering region is between  $r_{max}$  and  $2 r_{max}$ . For a constant  $PRF$ , the radar processing equipment is not able to distinguish between range  $r$  and ranges  $r + r_{max}$  (second trip),  $r + 2 r_{max}$  (third trip), or  $r + 3 r_{max}$  (fourth trip). Measurements from all trips are “folded” back into the first trip interval. Thus, all measured ranges are potentially ambiguous because, without additional information, it is not possible to determine the proper trip to which a returned signal should be assigned. Design of the WSR–88D and its scanning strategies permit range-folded Doppler velocity and spectrum width data to be recovered and placed into the proper range interval or trip (e.g., Doviak and Zrnić 1993, pp. 175–177). This may not be true for other Doppler radars.

The process of range folding is illustrated in Fig. 1.2.1 for a radar that is not able to recognize and resolve range-folded radar return. The radar is at the center of the circle having a radius of  $r_{max}$ . The hatched region surrounding the radar location represents return from the ground and objects such as trees and buildings. North of the radar, four irregular storm regions (labeled 1, 2, 3, 4) are in a line oriented from the west-southwest toward the east-northeast. The shaded regions represent radar return measured by the radar. Storms 1 and 4 beyond the  $r_{max}$  circle are folded to ranges within the circle (1' and 4'). For storm 2, which straddles the circle, only the outer portion (within the second-trip ground return region) is folded back to the radar location (2'). Note that second-trip radar echoes are narrower within the first-trip domain because echo angular width is maintained and thus the linear width approaches zero with decreasing distance from the radar.

*b. Concept of Doppler Velocity Aliasing*

One way to alleviate the range-folding problem is to decrease the  $PRF$  until  $r_{max}$  is beyond all scattering regions. However, this approach introduces an additional problem for Doppler radars. The maximum Doppler velocity measuring interval (called the Nyquist cointerval) is related to the  $PRF$  and the radar wavelength,  $\lambda$ , by

$$V_{max} = \pm PRF \lambda / 4 ; \tag{1.2.3}$$

see Battan (1973) for a derivation of this expression. As the  $PRF$  decreases,  $V_{max}$  decreases and a problem called Doppler velocity aliasing (analogous to range folding) occurs. Solving Eq. (1.2.3) for  $PRF$  and substituting it into Eq. (1.2.2), one finds that

$$V_{max} r_{max} = \pm c \lambda / 8 . \tag{1.2.4}$$

Thus, for a Doppler radar having a specific wavelength, the product of  $V_{max}$  and  $r_{max}$  is a constant; increasing  $r_{max}$  decreases  $V_{max}$  and vice versa. This unfortunate tradeoff between  $V_{max}$  and  $r_{max}$  frequently is referred to as the “Doppler dilemma” (e.g., Rinehart 2004).

The process of Doppler velocity aliasing is illustrated in Fig. 1.2.2. Consider a uniform wind blowing from the west at  $36 \text{ m s}^{-1}$  (70 kt) at a particular height in the atmosphere. As the radar antenna rotates  $360^\circ$  in azimuth, the Doppler velocity at a specified range gate location (at an elevated slant range at the height of the  $36 \text{ m s}^{-1}$  winds) varies as a sinusoidal curve as sketched in Fig. 1.2.2. Since a Doppler radar measures the component of wind relative to the radar viewing

direction, a Doppler velocity value of  $+36 \text{ m s}^{-1}$  (positive values representing flow away from the radar) occurs when the radar points toward the east ( $90^\circ$ ). When the radar points toward the west ( $270^\circ$ ), the Doppler velocity value is  $-36 \text{ m s}^{-1}$  (negative values representing flow toward the radar). When the radar points toward the north ( $0^\circ$ ) or south ( $180^\circ$ ), the Doppler velocity value is zero because the wind is perpendicular to the radar viewing direction.

When  $V_{max}$  is  $\pm 30 \text{ m s}^{-1}$  (58 kt), for example, and the environmental wind is  $36 \text{ m s}^{-1}$ , Doppler velocity values in excess of  $\pm 30 \text{ m s}^{-1}$  are aliased. The portions of the solid curves in Fig. 1.2.2 represent the Doppler velocity values measured by the radar. The aliasing process causes the true Doppler velocity values to be offset by multiples of  $2 V_{max}$  until they fall within the Nyquist cointerval. Thus,  $+36 \text{ m s}^{-1}$  is aliased to  $+36 - 2 \times 30 = -24 \text{ m s}^{-1}$  and  $-36 \text{ m s}^{-1}$  is aliased to  $-36 + 2 \times 30 = +24 \text{ m s}^{-1}$ ; in this case, the true values are offset by only one multiple of  $2 V_{max}$  in order to fall within the  $\pm 30 \text{ m s}^{-1}$  Nyquist cointerval.

Without additional information, it is not possible to determine whether an *individual* Doppler velocity data point has been aliased. However, spatial continuity (as in Fig. 1.2.2) permits one to readily identify visually the presence of aliasing and to make the proper adjustments. Computer algorithms are designed to objectively identify and correct aliased Doppler velocity data (e.g., Eilts and Smith 1990; Conway et al. 1995).

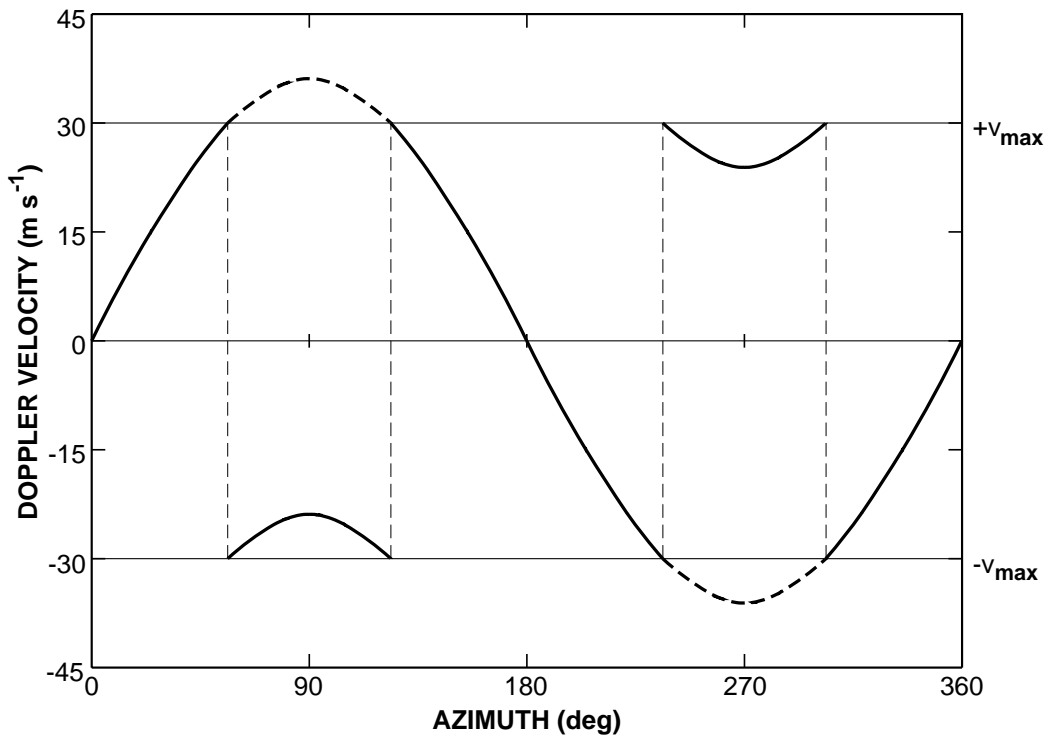


**Fig. 1.2.2.** Display of Doppler velocity at a given range gate as a function of azimuth when the radar antenna rotates at a fixed elevation angle. The sinusoidal curve represents true Doppler velocity measurements of a wind blowing from the west at  $36 \text{ m s}^{-1}$  (70 kt). The thick solid curves represent Doppler velocity values within the Nyquist cointerval of  $\pm 30 \text{ m s}^{-1}$  (58 kt).

### 1.3 Organization of This Guide

The Doppler velocity displays in this guide are simulated. The simulations are based on analytical functions similar to those used by Wood and Brown (1986) and Brown and Wood (1991). They also were inspired by simulated Doppler velocity patterns produced by Kraus and Donaldson (1976) and Baynton (1979), among others. The radar's beamwidth is assumed to be zero, such that there is no azimuthal smearing (degradation) of the simulated data; in reality, data degradation increases with increasing range because the linear width of the beam increases with range (angular width remains constant). Data are collected/digitized at 0.25 km (0.13 n mi) intervals in range and 1° intervals in azimuth, following the conventional sampling procedures of a WSR-88D.

In Chapter 2, simulated Doppler velocity patterns from widespread precipitation and clear air are presented on a plan position indicator (PPI) display that is a conical surface at a given elevation angle. In most cases, the wind is assumed to be horizontally homogeneous and to vary only in the vertical. But there are a few examples of more realistic wind fields where there are variations across the display. Small-scale noise and point-to-point random noise were added to the displays to give a semblance of reality.

In Chapter 3, simulated Doppler velocity patterns are presented of a tropical cyclone as it approaches a coastal radar. As the storm approaches, the Doppler velocity pattern becomes increasingly distorted.

In Chapter 4, simulated Doppler velocity patterns within convective storms are presented in blown-up windows located 100 km (54 n mi) due north of a radar; no noise was added to these data. Typical flow fields at various stages of development and altitudes within convective storms are simulated. The displays are blocky because the individual range gates are more evident than they are on the full PPI display. The horizontal wind field from which each simulated Doppler velocity display was produced also is presented.



## 2. INTERPRETATION OF DOPPLER VELOCITY PATTERNS IN CLEAR AIR AND WIDESPREAD PRECIPITATION

### 2.1 Introduction

In the absence of significant vertical motion, Doppler velocity patterns in widespread stratiform precipitation and in optically clear air represent the environmental wind field. Depending on season and time of day, coherent clear-air return can extend to ranges of 50–100 km (27–54 n mi) and to heights of 1–3 km (3–10 kft). For the simulations presented in this chapter, the wind is assumed to be uniform at each height but can vary from one height to the next; exceptions to this assumption are presented in Section 2.3. The assumption of horizontal uniformity is a realistic approximation to real data.

For a Doppler radar scanning  $360^\circ$  at a given elevation angle (Fig. 2.1.1), distance radially outward along the radar beam represents increasing height above the ground (really height above the center of the radar antenna). Thus, when the environmental wind field varies only with height, one  $360^\circ$  scan of the radar reveals winds at all heights from the ground up through the height of the edge of the radar scope display (for clear air, through the shallower depth of coherent radar return).

An example of an environmental wind field and corresponding color display of Doppler velocity values is shown in Figs. 2.1.2a and b. Since the choice of color scheme is based on personal preference, we chose contrasting colors that are obvious to those who cannot easily distinguish between reds and greens. The wind field is the same ( $26 \text{ m s}^{-1}$  or 50 kt) at all heights. The wind direction changes uniformly from southerly at the ground (center of display) to westerly at the height of the edge of the display. Figure 2.1.2c indicates how to interpret wind direction along the gray zero Doppler velocity curve. The presence of the zero value indicates that the wind direction is perpendicular to the radial viewing direction from the radar at that location. For

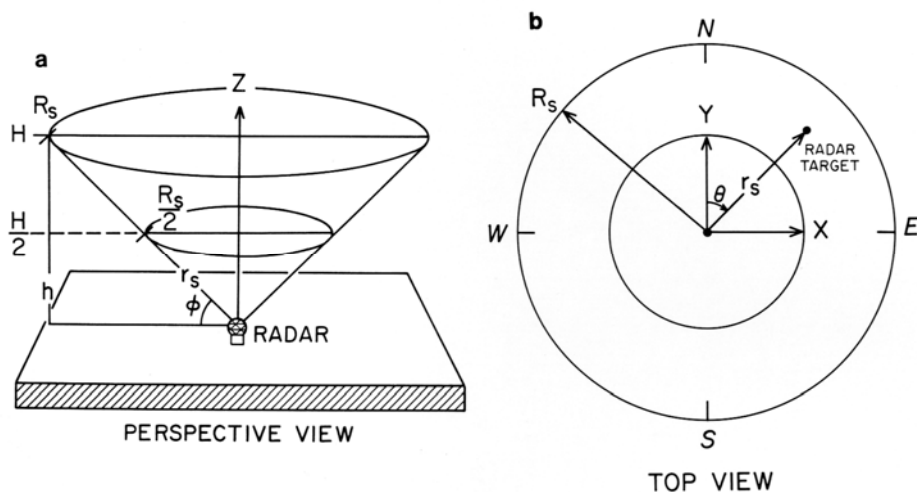


**Fig. 2.1.1.** Doppler radar viewing configuration. (a) Radar scanning around vertical axis,  $Z$ , at a constant elevation angle,  $\phi$ ; (b) view of (a) from the top, representing a PPI (plan position indicator) display.  $R_s$  is slant range (on conical surface) of the edge of the display corresponding to height  $H$  above the ground. The three-dimensional position  $(x, y, h)$  of a radar scattering volume (“target”) is computed from radar azimuth angle  $\theta$ , elevation angle  $\phi$ , and slant range  $r_s$ .

example, along the outer edge of the display, the Doppler velocity is zero when the radar points toward the north (point 1) and the south (point 7). This means that the wind is blowing either from west to east or from east to west at the height corresponding to the edge of the display. Since Doppler velocities are negative (component toward the radar) along the western edge of the display and positive (component away from the radar) along the eastern edge, the wind obviously is blowing from west to east at the height of the edge of the display.

When the radar points toward point 2 on the zero band, it is pointing toward  $330^\circ$ . The wind direction at that point is  $330^\circ \pm 90^\circ$ . Since the wind is blowing generally from west to east, the wind at point 2 must be from  $330^\circ - 90^\circ = 240^\circ$ . Similar arguments at points 3, 5, and 6 result in wind direction of  $300^\circ - 90^\circ = 210^\circ$ ,  $120^\circ + 90^\circ = 210^\circ$ , and  $150^\circ + 90^\circ = 240^\circ$ , respectively. At the radar location on the ground (point 4) the zero band is oriented east-west. Since the wind at the surface is approaching the radar from the south, the wind is blowing from  $180^\circ$ .

Wind speed at a given height (slant range) is determined by the extreme Doppler velocity values around a constant slant range circle (as displayed in Fig. 1.2.2). In Fig. 2.1.2b, the maximum flow away from the radar (light orange) and the maximum flow toward the radar (light blue) is the same from the center out to the edge of the display, indicating that the wind speed is constant (between  $25$  and  $30 \text{ m s}^{-1}$ ) from the ground to the height corresponding to the edge of the display. Thus the Doppler velocity pattern in Fig. 2.1.2b uniquely represents an environmental wind profile where wind speed is constant and wind direction veers uniformly from southerly at the ground through southwesterly to westerly at the edge of the display.

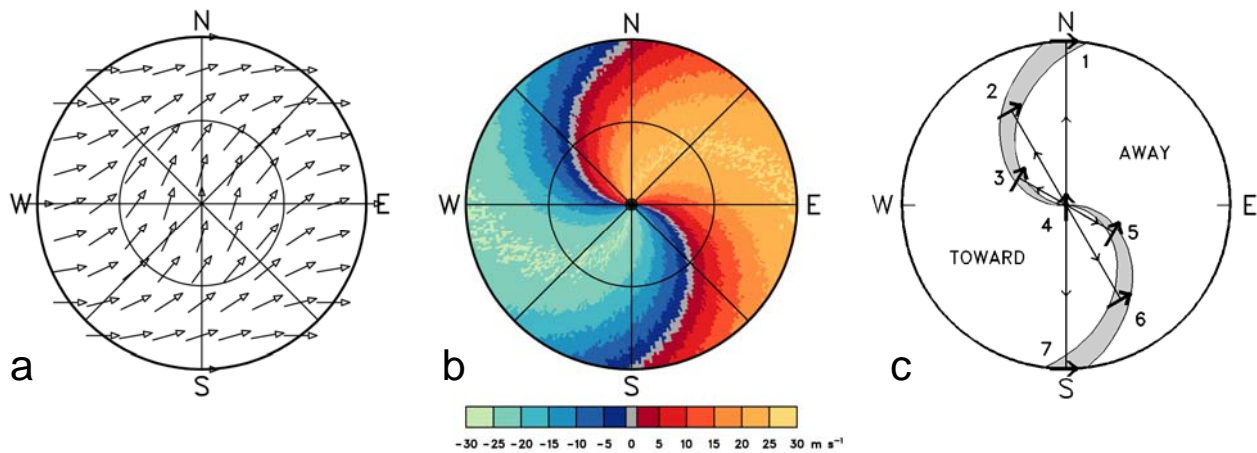


**Fig. 2.1.2.** Plan view of (a) environmental wind field and (b) corresponding single Doppler velocity pattern for wind with constant speed ( $26 \text{ m s}^{-1}$  or  $50 \text{ kt}$ ) and with direction changing uniformly from southerly at the ground (center of display) through southwesterly to westerly at the edge of the display. Part (c) illustrates how wind direction in a horizontally homogenous flow field can be interpreted using the zero Doppler velocity band. Uniform arrow length in (a) indicates constant wind speed with height. Colors in (b) indicate Doppler velocity values: positive values (red and orange) present flow away from the radar, negative values (blues) represent flow toward the radar. The lightest blue color category represents velocities  $< -25 \text{ m s}^{-1}$  and the lightest orange category represents velocities  $> +25 \text{ m s}^{-1}$ .

## 2.2 Patterns Associated with Vertical Profiles having Constant Wind Direction

Doppler velocity patterns associated with the same wind direction at all heights always have a straight zero band. The rest of the pattern reflects the vertical profile of wind speed (Figs. 2.2.1–2.2.4).

When wind speed is constant (non-zero) with height (Fig. 2.2.1), the extreme Doppler velocity values extend from the radar location at the center (ground level) outward to the edge of the display. Consequently, the colors representing all other Doppler velocity values must converge to a point at the display center.

When wind speed at the ground is less than the maximum value (but still greater than zero), those colors corresponding to wind speeds less than or equal to the surface value converge to the center of the display (Figs. 2.2.2 and 2.2.3). Those colors corresponding to greater speeds converge toward the center but never reach it. When wind speed at the ground is zero, only the zero band passes through the center (Fig. 2.2.4).

When a wind speed maximum exists within the height interval represented by the display, a pair of quasi-elliptical bull's eyes appear on the display (Figs. 2.2.3 and 2.2.4). The centers of the bull's eyes are positioned upwind (negative) and downwind (positive) of the radar at the slant range equal to the height of the wind maximum.

**Note:** The plotted wind barbs presented in this guide follow the customary convention: a short barb represents 5 kt ( $2.6 \text{ m s}^{-1}$ ), a long barb represents 10 kt ( $5.1 \text{ m s}^{-1}$ ), and a flag represents 50 kt ( $26 \text{ m s}^{-1}$ ). The barbs and flags point toward lower pressure.

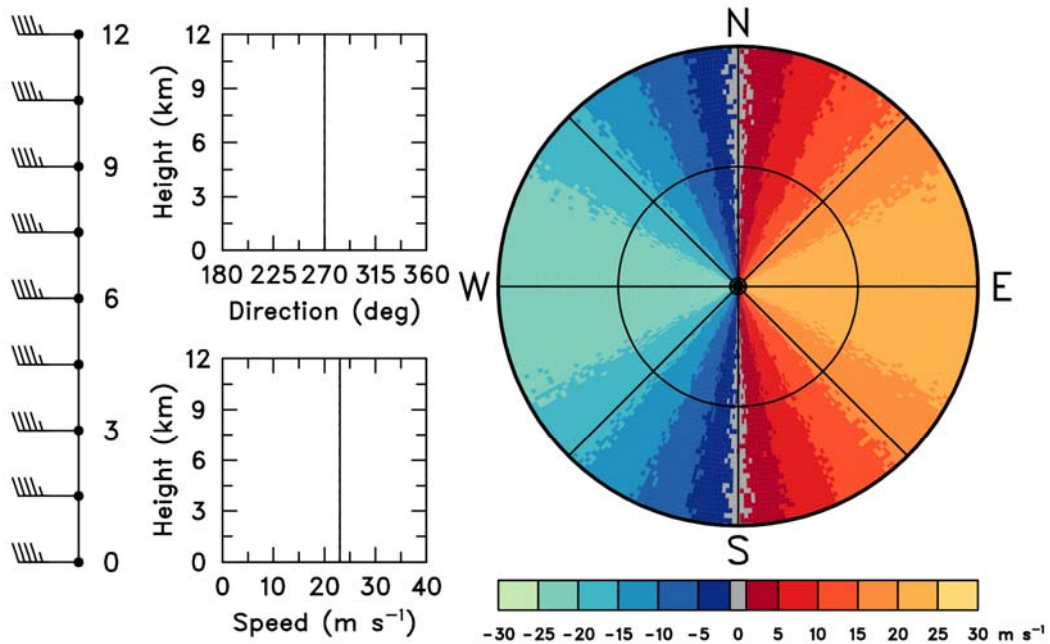


**Fig. 2.2.1.** Doppler velocity pattern (right) corresponding to a vertical wind profile (left) where both speed ( $23 \text{ m s}^{-1}$  or  $45 \text{ kt}$ ) and direction ( $270^\circ$ ) are constant with height. Negative (positive) Doppler velocities represent flow toward (away from) radar. Radar is at the center of the display.

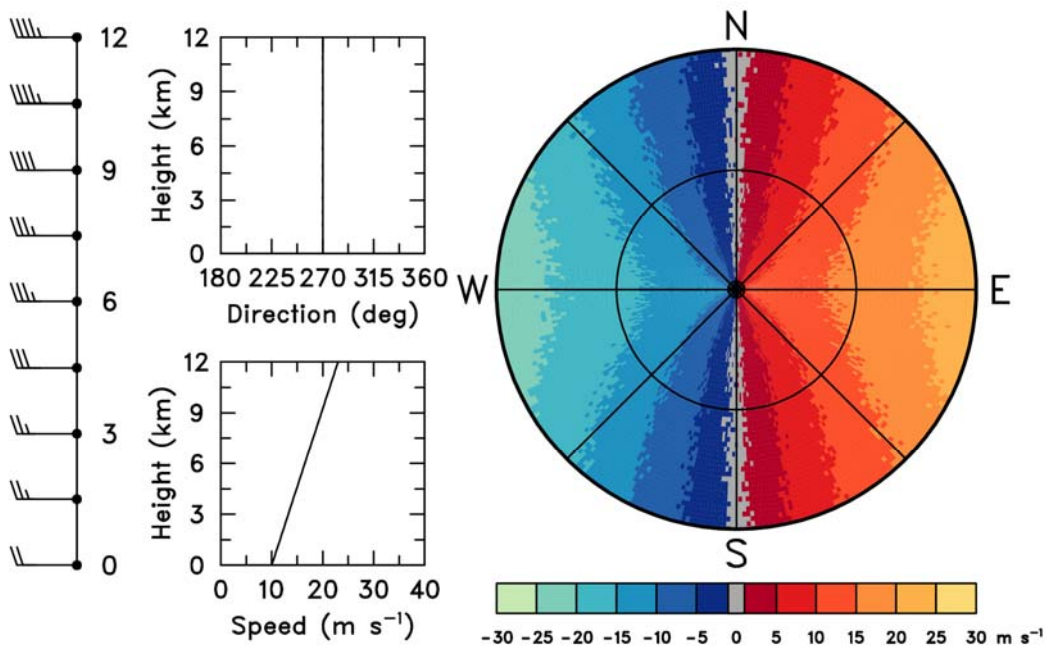


**Fig. 2.2.2.** Same as Fig. 2.2.1, except that the wind speed increases from  $10 \text{ m s}^{-1}$  ( $19 \text{ kt}$ ) at the ground to  $23 \text{ m s}^{-1}$  ( $45 \text{ kt}$ ) at the edge of the display.

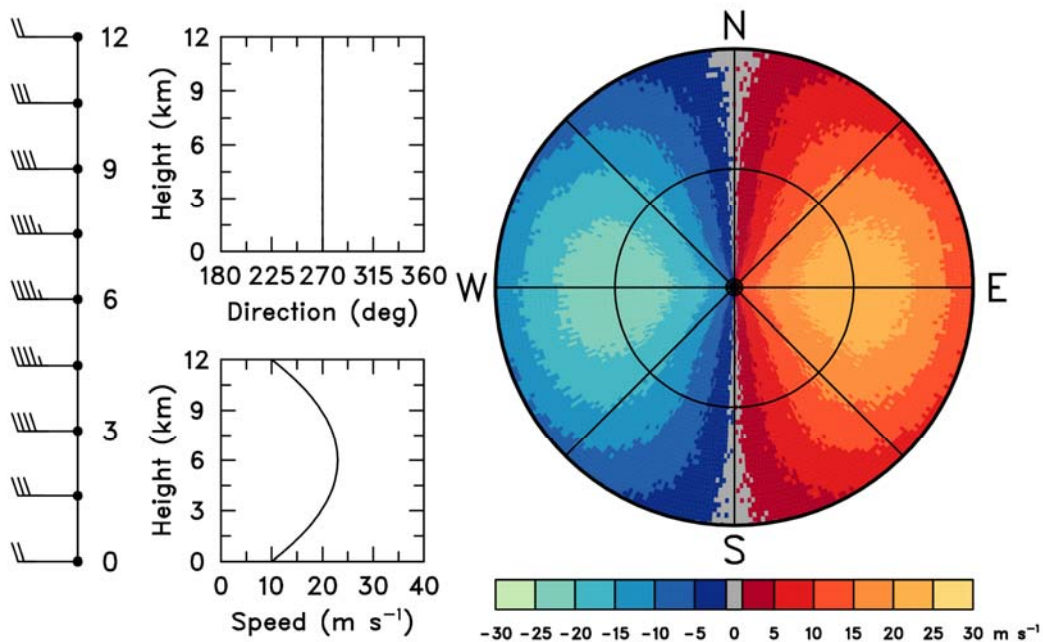


**Fig. 2.2.3.** Same as Fig. 2.2.1, except that the wind speed is a maximum of  $23 \text{ m s}^{-1}$  (45 kt) midway between the ground and the height corresponding to the edge of the display. Speed is  $10 \text{ m s}^{-1}$  (19 kt) at the surface and at the edge of the display.

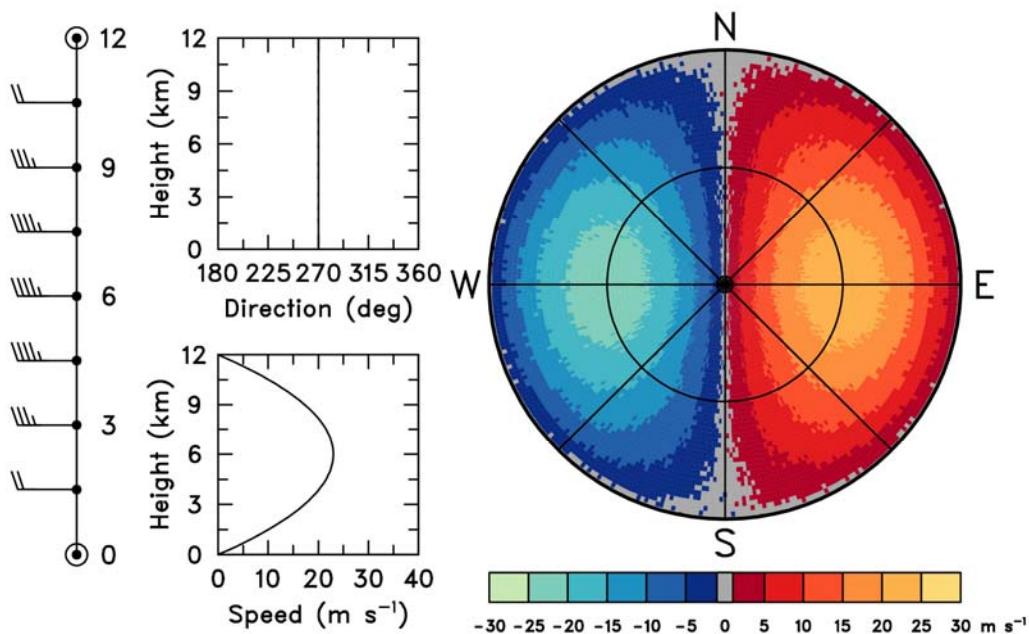


**Fig. 2.2.4.** Same as Fig. 2.2.3, except that wind speed is zero at the ground and at the edge of the display.

### 2.3 Patterns Associated with Nonuniform Horizontal Wind Fields

Everywhere else in this chapter, it is assumed that the environmental wind field is horizontally uniform. However, in this section, we explore some nonuniform features as discussed by Baynton et al. (1977). In Figs. 2.3.1 and 2.3.2, the horizontal winds at all heights are horizontally diffluent and confluent, respectively. The straight velocity boundaries of Fig. 2.2.1 become curved, with the curve of the zero Doppler velocity line reflecting the change in wind direction across the display.

When the height of the wind speed maximum profile in Fig. 2.2.4 increases toward the east, variations in the wind profiles are like those shown in the left part of Fig. 2.3.3. The profile labeled W represents the wind in the western half of the display and the profile labeled E represents the wind in the eastern half of the display. The Doppler velocity display consists of an unsymmetrical bull's eye pattern representing the upward tilt of the maximum wind speed structure from west to east.

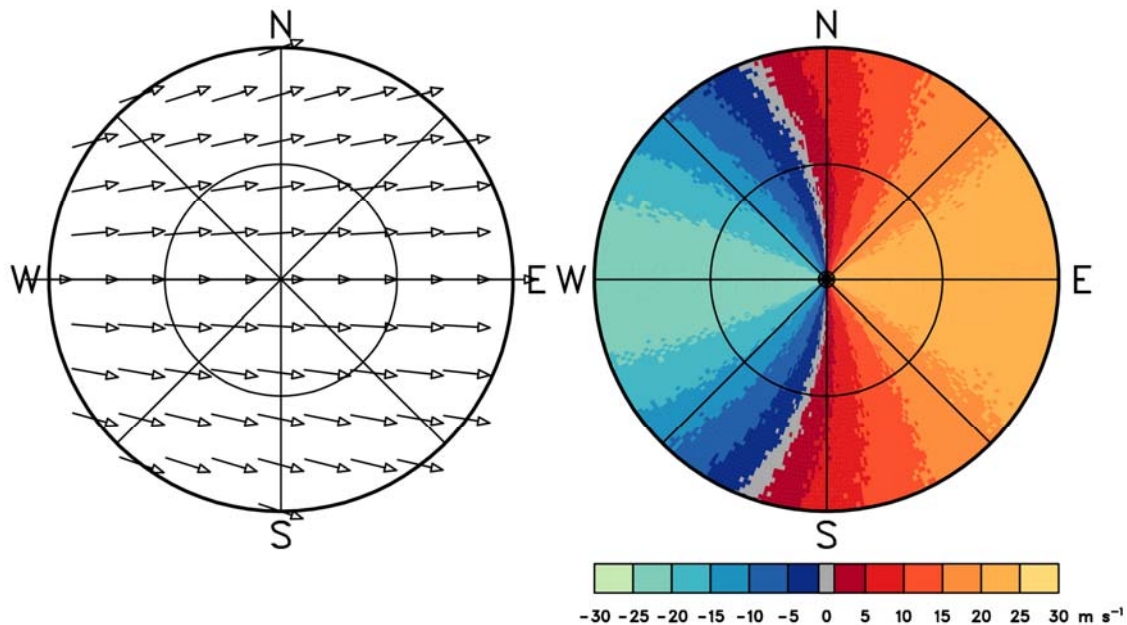


**Fig. 2.3.1.** Doppler velocity pattern (right) corresponding to a horizontal flow field that is diffluent with the same speed ( $23 \text{ m s}^{-1}$  or 45 kt) at all heights (left). Negative (positive) Doppler velocities represent flow toward (away from) the radar. Radar location is at the center of the display.

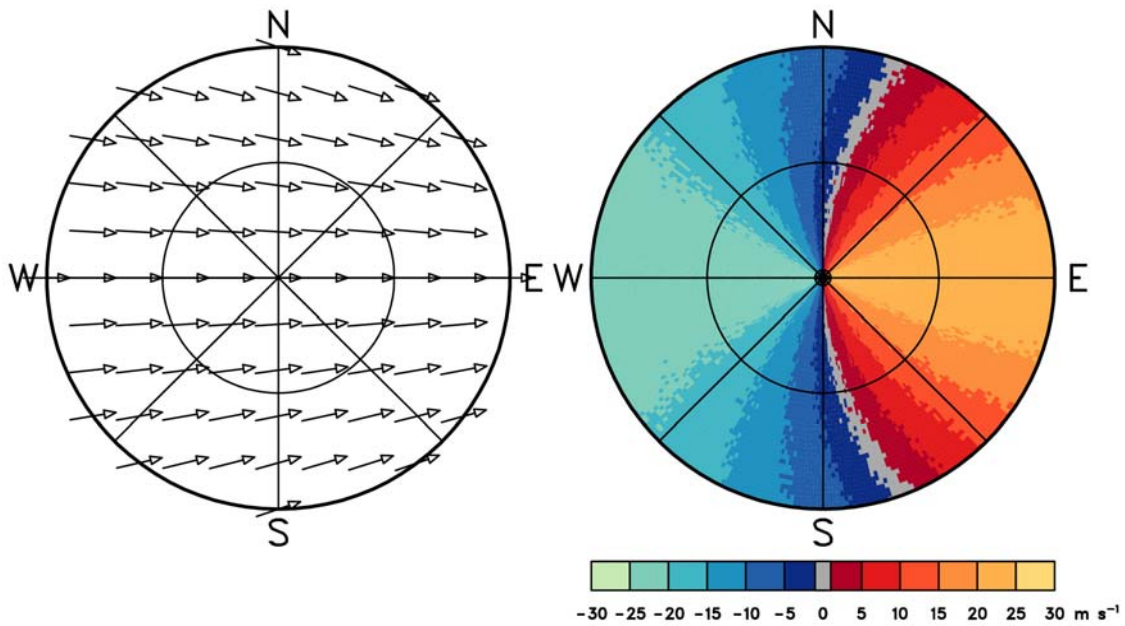


**Fig. 2.3.2.** Same as Fig. 2.3.1, except that the horizontal flow field is confluent with the same speed ( $23 \text{ m s}^{-1}$  or 45 kt) at all heights.

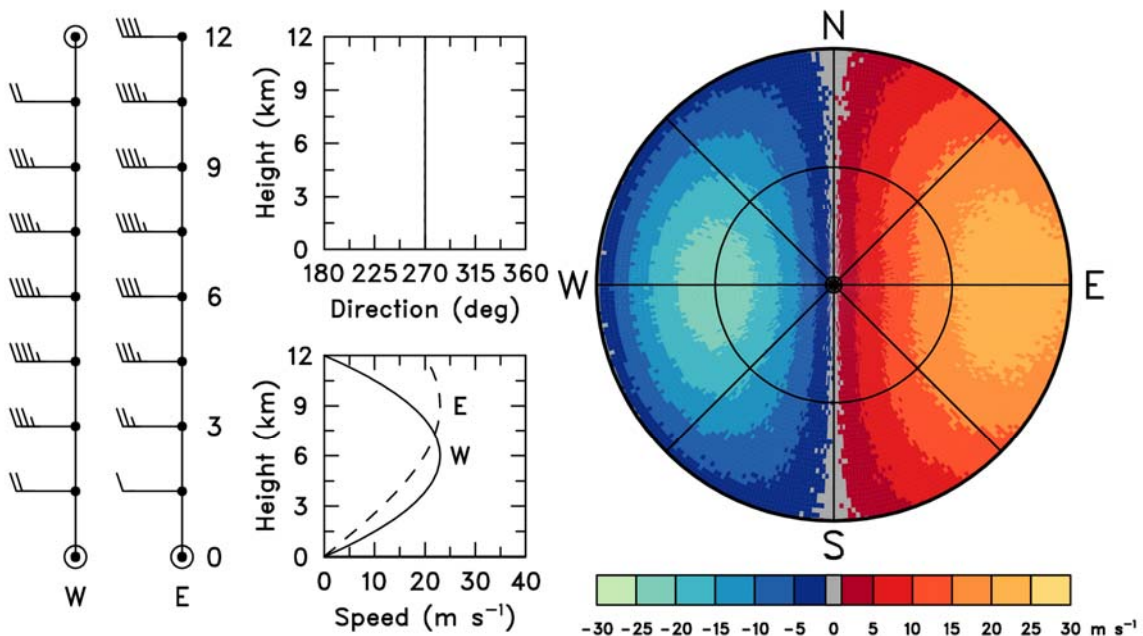


**Fig. 2.3.3.** Doppler velocity pattern (right) corresponding to a wind speed pattern (left) similar to that in Fig. 2.2.4 that tilts upward from west (*W*) to east (*E*).

## 2.4 Patterns Associated with Vertical Profiles having Constant Wind Speed

When wind speed is constant with height, all of the color velocity bands converge to the radar location at the center of the display. Curvature of the zero Doppler velocity line indicates the change of wind direction with height (see Fig. 2.1.2). *Backing* winds produce a *backward* S-shaped profile (Fig. 2.4.1) and veering winds produce an S-shaped profile (Fig. 2.4.2). When the wind direction veers then backs with height, an S-shaped profile changes into a backward S-shaped profile with increased range from (height above) the radar (Fig. 2.4.3).

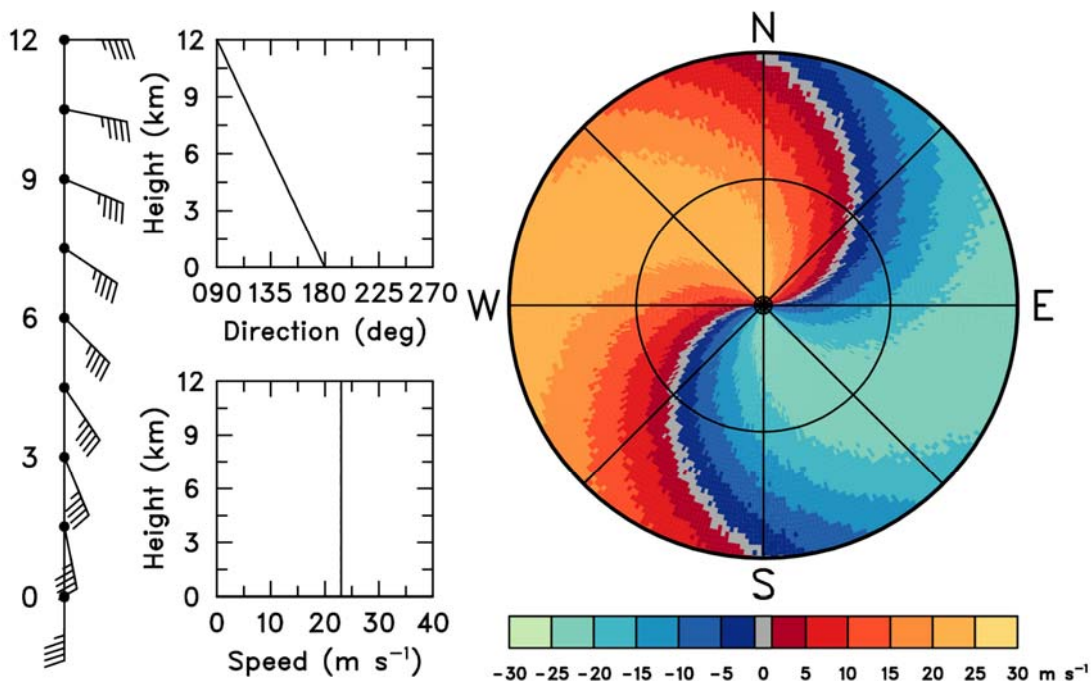


**Fig. 2.4.1.** Doppler velocity pattern (right) corresponding to a vertical wind profile (left) with constant wind speed ( $23 \text{ m s}^{-1}$  or 45 kt) and wind direction backing from southerly to easterly with height. Negative (positive) Doppler velocities represent flow toward (away from) the radar. Radar location is at the center of the display.

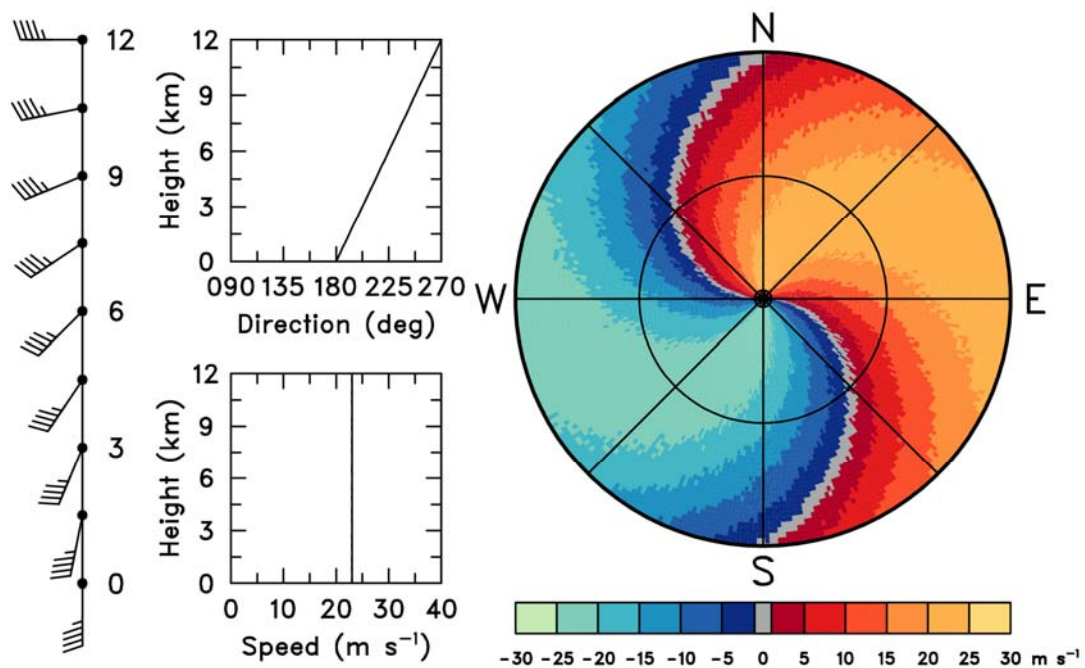


*Fig. 2.4.2. Same as Fig. 2.4.1, except that the wind veers with height.*

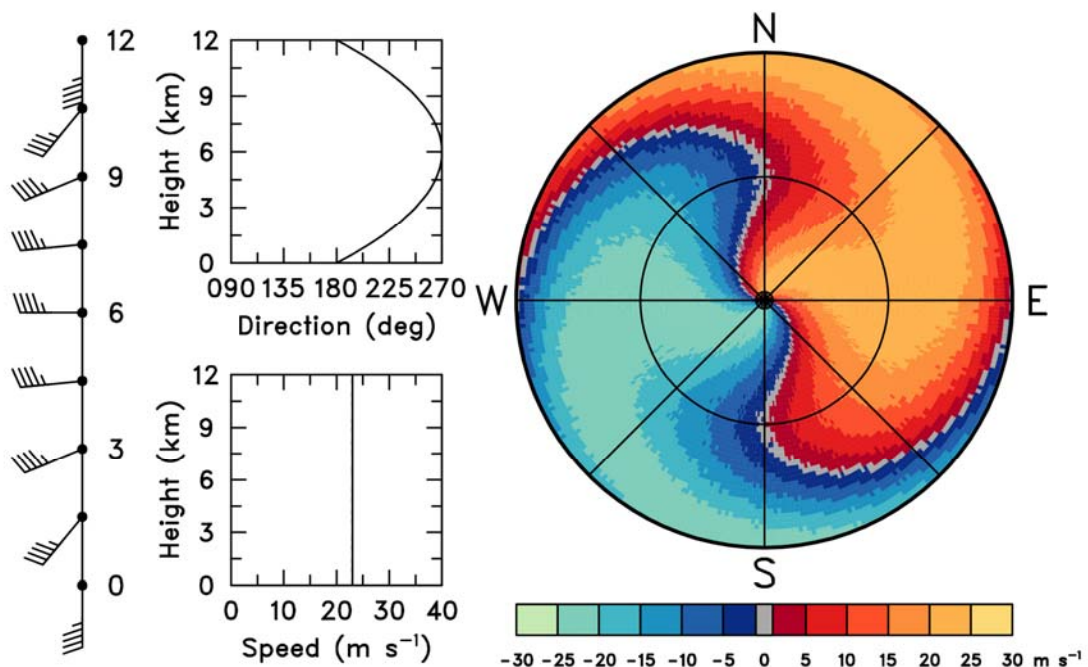


*Fig. 2.4.3. Same as Fig. 2.4.1, except that the wind direction veers then backs with height.*

## 2.5 Patterns Associated with Vertical Profiles of Varying Wind Speed and Direction

A wide variety of Doppler velocity patterns are possible when both wind speed and direction vary with height. Figure 2.5.1 shows a variation of Fig. 2.4.2, where wind direction veers with height but where the speed increases with height instead of being constant. Since wind speed is zero at the ground in Fig. 2.5.1, only the zero velocity line passes through the radar location at the center of the display.

If the Doppler velocity dealiasing algorithm is not applied or is not functioning properly, Doppler velocity values that exceed the Nyquist velocity cointerval will produce an abrupt change in color from one end of the velocity cointerval to the other. This abrupt color change makes the presence of velocity aliasing very evident to the eye. In the example shown in Fig. 2.5.1, the Doppler velocities at the edges of the display are aliased because the wind speeds at those heights exceed an assumed Nyquist velocity cointerval of  $\pm 30 \text{ m s}^{-1}$  (58 kt).

When wind speed at the ground is greater than zero, color bands for velocities less than or equal to the surface wind speed converge to the center of the display (Fig. 2.5.2). The presence of a wind speed maximum aloft produces bull's eyes that are distorted due to the change of wind direction with height (Fig. 2.5.3). Note that all three of the Doppler velocity displays have aliased Doppler velocity values.

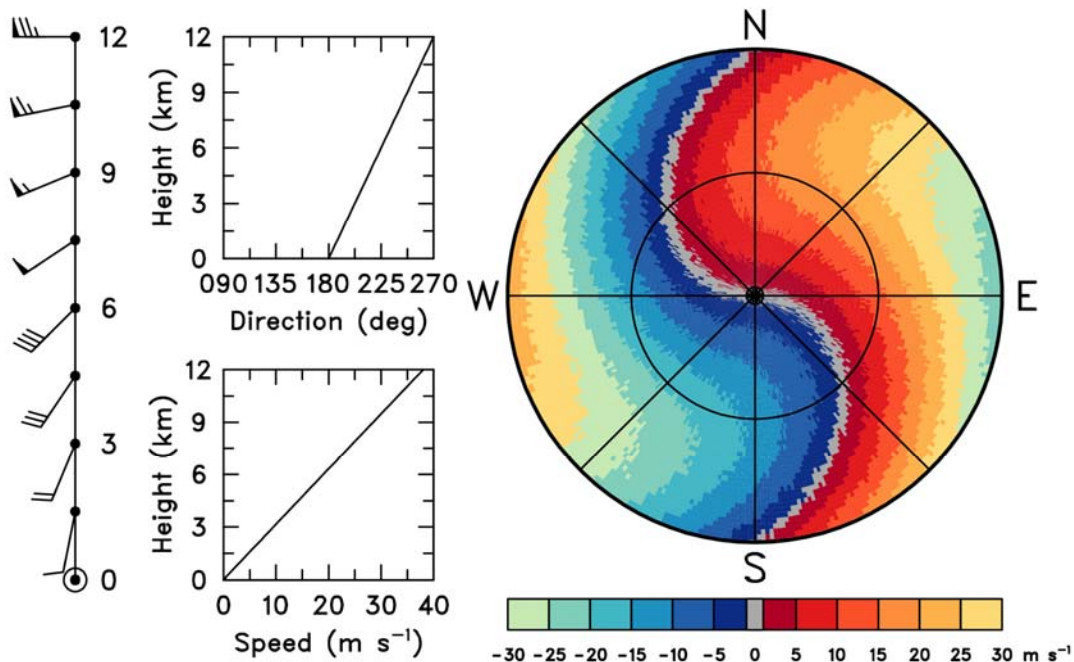


**Fig. 2.5.1.** Doppler velocity pattern (right) corresponding to a vertical wind profile (left) where wind speed increases from  $0$  to  $38 \text{ m s}^{-1}$  (74 kt) and direction veers from southerly to westerly with height. Negative (positive) Doppler velocities represent flow toward (away from) the radar. Note that Doppler velocities exceeding  $\pm 30 \text{ m s}^{-1}$  are aliased.

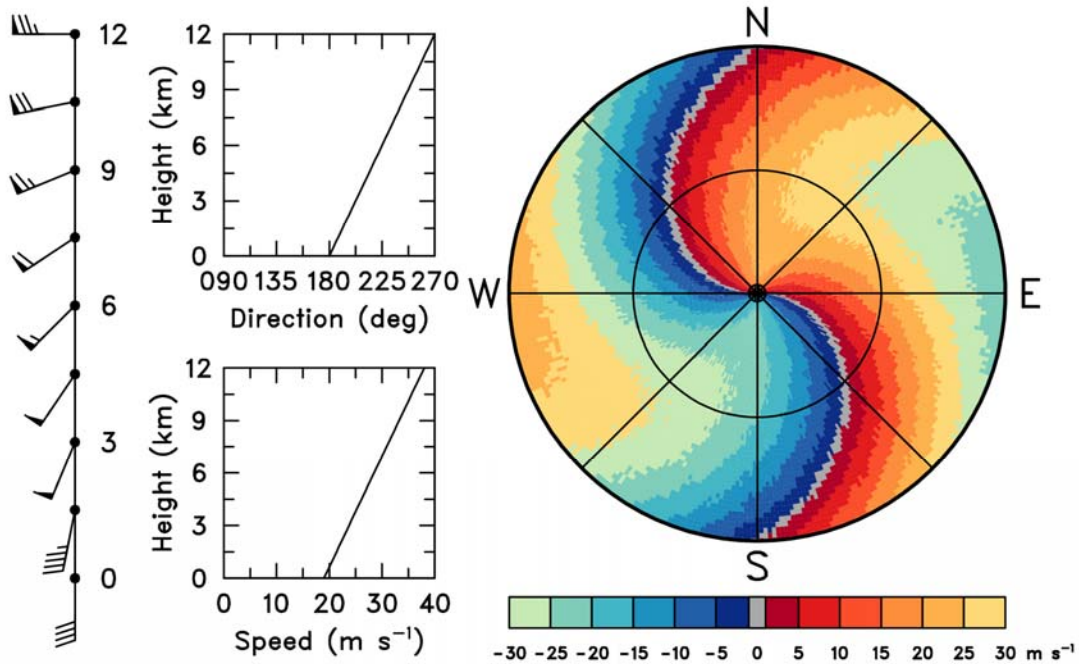


**Fig. 2.5.2.** Same as Fig. 2.5.1, except that the wind speed increases from  $19 \text{ m s}^{-1}$  (37 kt) at the ground to  $38 \text{ m s}^{-1}$  (74 kt) at the edge of the display.

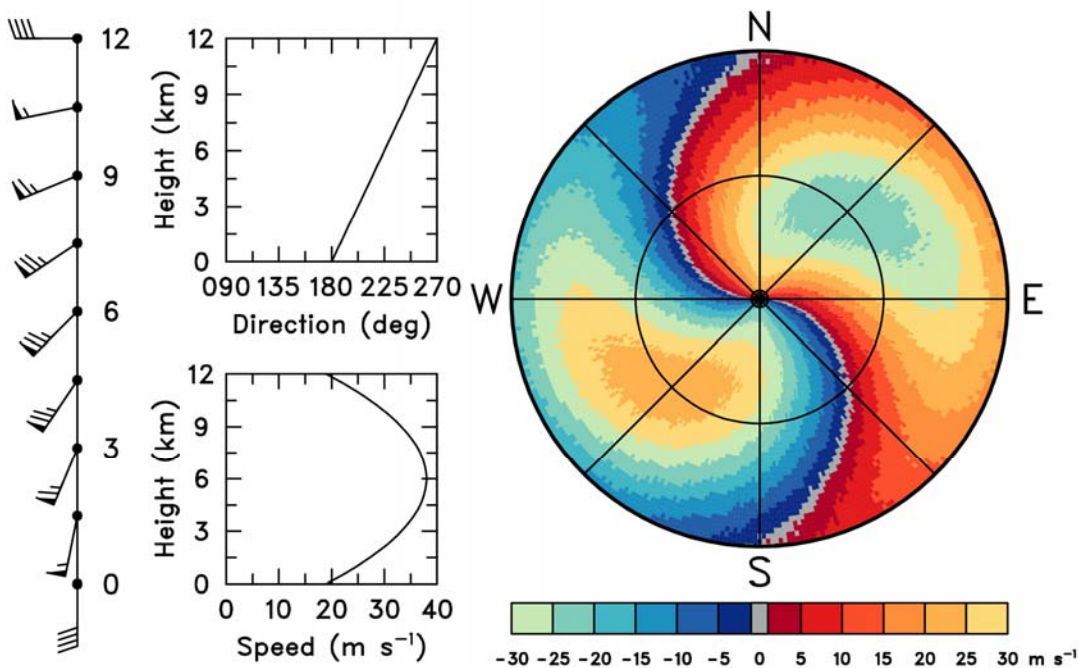


**Fig. 2.5.3.** Same as Fig. 2.5.2, except that the wind speed maximum of  $38 \text{ m s}^{-1}$  (74 kt) occurs at a height corresponding to the midrange of the display and decreases to  $19 \text{ m s}^{-1}$  (37 kt) at the edge.

## 2.6 Patterns Associated with Vertical Discontinuities in the Wind Field

Figures 2.6.1 and 2.6.2 illustrate examples of Doppler velocity fields that pass through a horizontal surface that separates two different atmospheric flow regimes. It is assumed that there is a wind speed maximum within each wind regime and that the wind directions differ by  $90^\circ$  or  $180^\circ$ , respectively, across the discontinuity.

The discontinuity could represent a frontal surface or it could represent the top of the boundary layer in clear air. Note the variation of the zero Doppler velocity line in Fig. 2.6.1. It is oriented northeast-southwest through the center of the display indicating a constant wind direction in the lower layer. The inner pair of bull's eyes indicates that the wind is blowing from the southeast to northwest at a maximum speed of  $25\text{--}30\text{ m s}^{-1}$  (49–58 kt). The zero velocity line indicates a  $90^\circ$  shift in wind direction through a narrow height interval, with the wind direction becoming constant again above the discontinuity. The second pair of bull's eyes indicates that the upper layer winds are from the southwest at a maximum speed of  $25\text{--}30\text{ m s}^{-1}$  (49–58 kt).

The wind shift through the discontinuity is much more dramatic in Fig. 2.6.2 than in Fig. 2.6.1. The orientation of the zero Doppler velocity line and the locations of the positive and negative Doppler velocity extremes indicate easterly winds in the lower layer capped by westerly winds aloft.

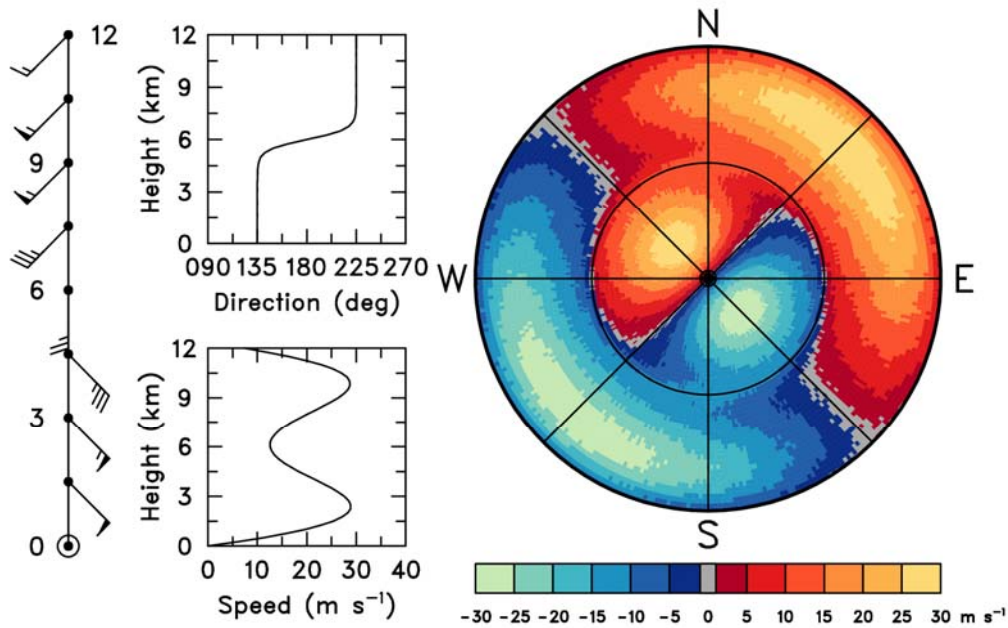


**Fig. 2.6.1.** Doppler velocity pattern (right) corresponding to a vertical wind profile (left) through a discontinuity between two wind regimes that differ by  $90^\circ$  in direction. Negative (positive) Doppler velocities represent flow toward (away from) the radar. Radar location is at the center of the display.

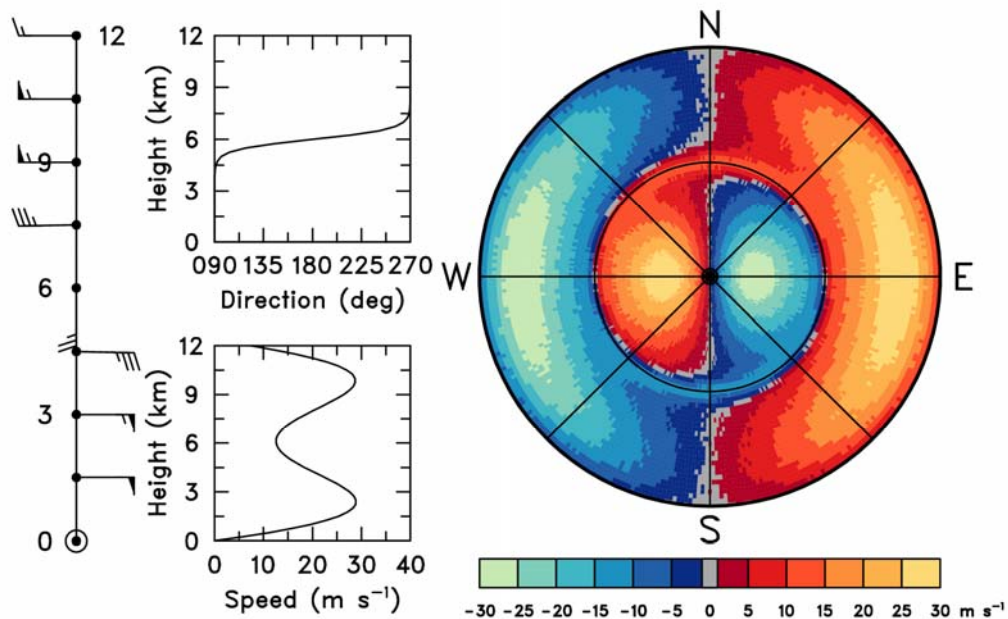


**Fig. 2.6.2.** Doppler velocity pattern (right) corresponding to a vertical wind profile (left) through a discontinuity between two wind regimes that differ by  $180^\circ$  in direction.

## 2.7 Patterns Associated with Horizontal Discontinuities in the Wind Field

With adequate radar return, it is possible to determine characteristics of the flow field both ahead of and behind a horizontal discontinuity (such as a front, outflow boundary, wind shift line). Figures 2.7.1–2.7.3 clearly indicate that the discontinuity is marked by a rapid change of Doppler velocity values over a narrower transition region. The sequence of three figures shows the movement of the discontinuity approaching from the northwest, located over the radar, and finally moving away from the radar toward the southeast. Winds ahead of the discontinuity essentially are from the southwest and those behind the discontinuity essentially are from the northwest.

Different wind profiles are used in each figure. The variation in wind vectors is due to the change of wind with height. In Fig. 2.7.1, wind direction is constant on both sides of the discontinuity and wind speed is a maximum in the middle of the height interval (as in Fig. 2.2.3). Wind direction is constant on both sides of the discontinuity in Fig. 2.7.2, but wind speed increases linearly from the ground to the edge of the display (as in Fig. 2.2.2). In Fig. 2.7.3, wind speed increases with height from zero at the ground while wind direction veers ahead of the discontinuity (similar to Fig. 2.5.1) and backs behind it.

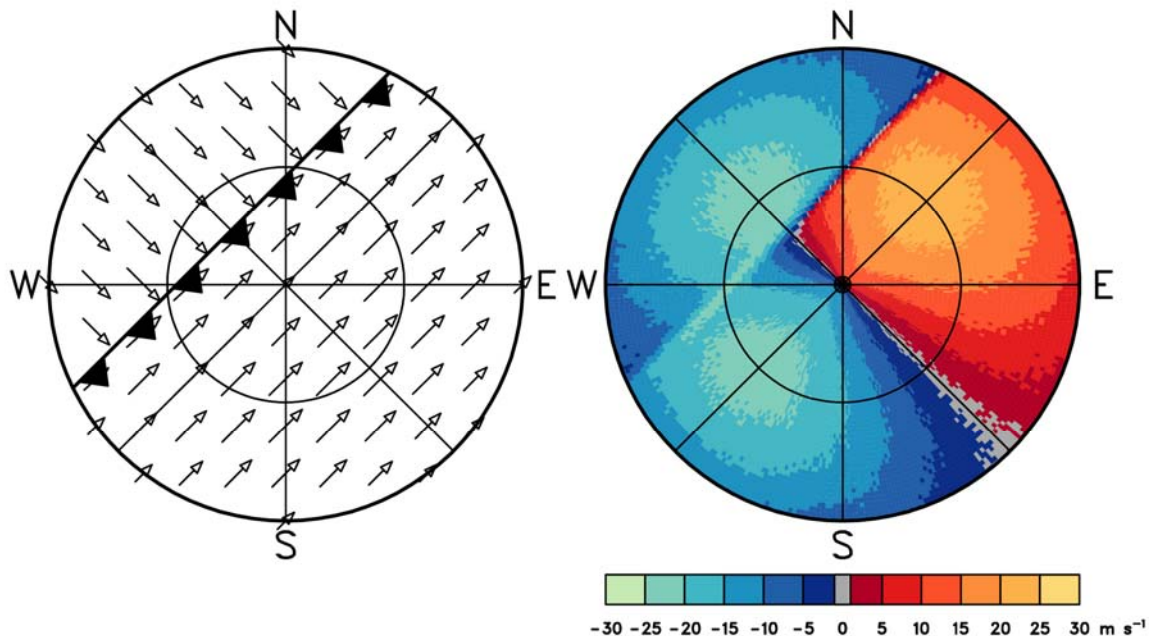


**Fig. 2.7.1.** Doppler velocity pattern (right) corresponding to the approach of a wind field discontinuity from the northwest (left). There is a southwesterly low-altitude velocity maximum of  $22 \text{ m s}^{-1}$  (43 kt) ahead of the discontinuity and a northwesterly velocity maximum of  $22 \text{ m s}^{-1}$  (43 kt) behind it. Wind speed at the ground is  $11 \text{ m s}^{-1}$  (21 kt). Arrow length is proportional to wind speed. Negative (positive) Doppler velocities represent flow toward (away from) the radar. Radar location is at the center of the display.

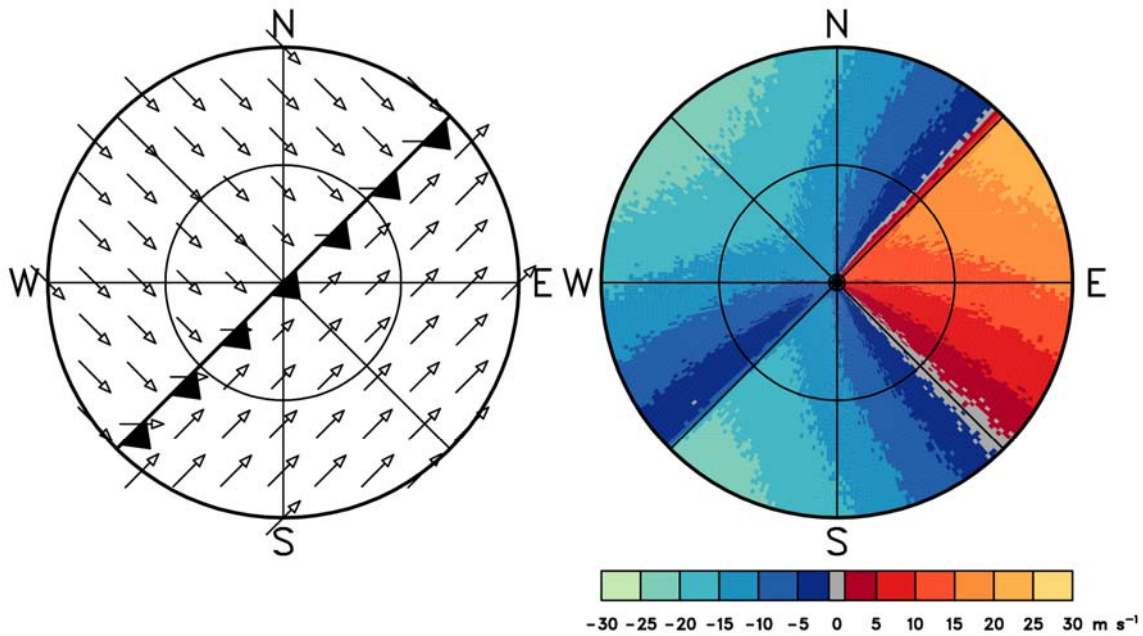


**Fig. 2.7.2.** Same as Fig. 2.7.1, except that the discontinuity is now over the radar. In both regions, wind direction is constant and wind speed increases from  $11 \text{ m s}^{-1}$  (21 kt) at the ground to  $22 \text{ m s}^{-1}$  (43 kt) at the edge of the display.

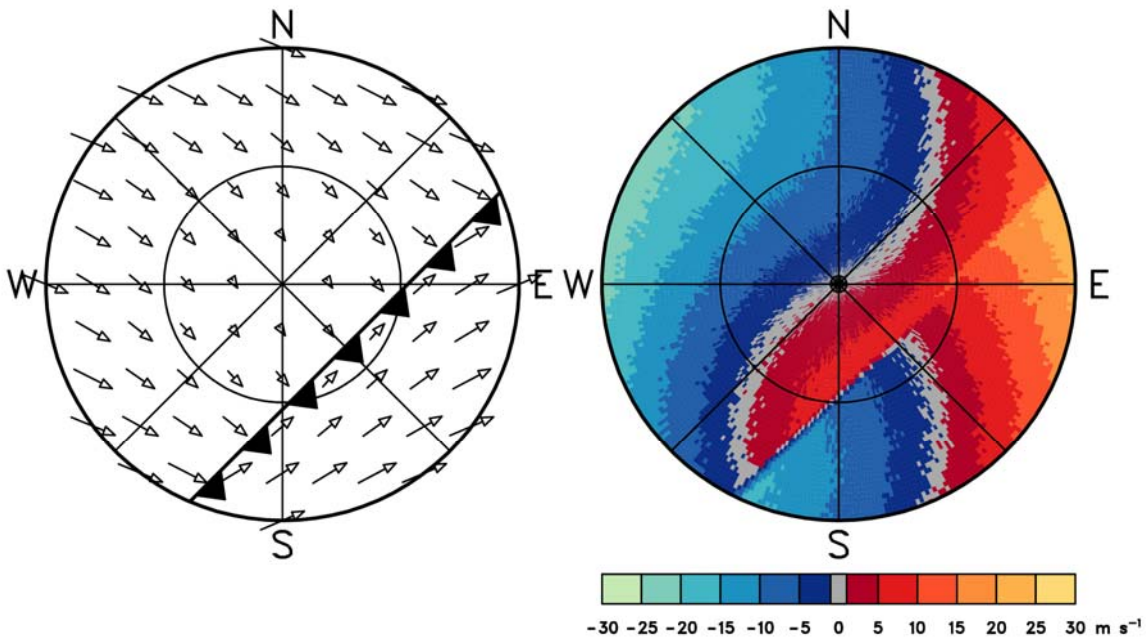


**Fig. 2.7.3.** Same as Fig. 2.7.1, except that the discontinuity is now southeast of the radar. Winds ahead of the discontinuity veer with height, while those behind the discontinuity back with height. In both regions, wind speed increases from  $0 \text{ m s}^{-1}$  at the ground to  $22 \text{ m s}^{-1}$  (43 kt) at the edge of the display.

### 3. INTERPRETATION OF DOPPLER VELOCITY PATTERNS WITHIN TROPICAL CYCLONES

Until the advent of weather satellites, conventional weather radars on the coasts and occasional reconnaissance aircraft penetrations provided the primary means for tracking the movement of tropical cyclones as they approached land. When satellites became available, the tracking capability was extended back to the point of origin and thus it became possible to monitor the evolution of tropical cyclones for many days as they moved toward land. Conventional radars and satellites provide general clues about storm strength and reconnaissance aircraft provide periodic estimates of maximum wind speeds. However, it was not until WSR-88D Doppler radars became operational in the early 1990s that one could continuously measure the maximum speeds within a storm as it approached the coastline.

In this chapter, we discuss how the storm-relative Doppler velocity pattern in a tropical cyclone changes as distance from the radar decreases. In order to present the basic features, we make a number of simplifying assumptions. We assume that the Doppler velocity pattern is due only to flow rotating around the cyclone center—axisymmetric and approximated by a Rankine combined vortex. A Rankine combined vortex consists of two regions: within the core region, tangential velocity increases linearly from zero at the center to the maximum speed at the edge of the core region; beyond the core region, tangential velocity changes (decreases) inversely proportional to distance from the circulation center. In order to depict changes in circulation appearance that are due only to changes in range, we further assume that the circulation structure is constant with height. Lastly, we assume that radar reflectivity is uniform across the tropical cyclone; with the absence of spiral rainbands, one is able to view the entire circulation without any of it missing owing to the lack of reflectivity.

Shown in Figs. 3.1–3.3 are simulated tropical cyclones at decreasing distances from a coastal Doppler radar. The maximum rotational velocity of  $60 \text{ m s}^{-1}$  (117 kt) occurs at a radius of 25 km (13.5 n mi) from the circulation center. Because the Nyquist velocity is only  $\pm 30 \text{ m s}^{-1}$ , the peak Doppler velocity values of both  $+60$  and  $-60 \text{ m s}^{-1}$  are aliased to  $0 \text{ m s}^{-1}$  (for example,  $60 \text{ m s}^{-1} - 2 \times 30 \text{ m s}^{-1} = 0 \text{ m s}^{-1}$ ). Since a Doppler radar measures only the component of motion toward or away from the radar, the Doppler velocity signature of an axisymmetric circulation includes zero Doppler velocity in the radial direction from the radar through the circulation center where flow is perpendicular to the radar viewing direction. As discussed in section 2.2, wind speed on the ground at the radar location is equal to the highest Doppler velocity contour that passes through the radar location. With the simulated cyclone 160 km from the radar (Fig. 3.1), the estimated surface wind speed at the radar site is  $5\text{--}10 \text{ m s}^{-1}$  (10–19 kt); at 80 km range (Fig. 3.2), it is  $15\text{--}20 \text{ m s}^{-1}$  (29–39 kt); and at 30 km range (Fig. 3.3), it is about  $50 \text{ m s}^{-1}$  (97 kt).

Peak Doppler velocity values occur at the edge of the core region where the radial viewing direction is tangent to the circle of maximum wind. As a tropical cyclone moves toward the radar, the points where radial lines are tangent to the circle (location of maximum wind) move closer together on the side of the core region nearer the radar (e.g., Wood and Brown 1992). This trait becomes apparent at 80 km range (Fig. 3.2) and is very obvious at 30 km range (Fig. 3.3). Even though the Doppler velocity pattern becomes increasingly distorted as the cyclone moves toward the radar, the peak Doppler velocity value is unaffected until the core region is over the radar.

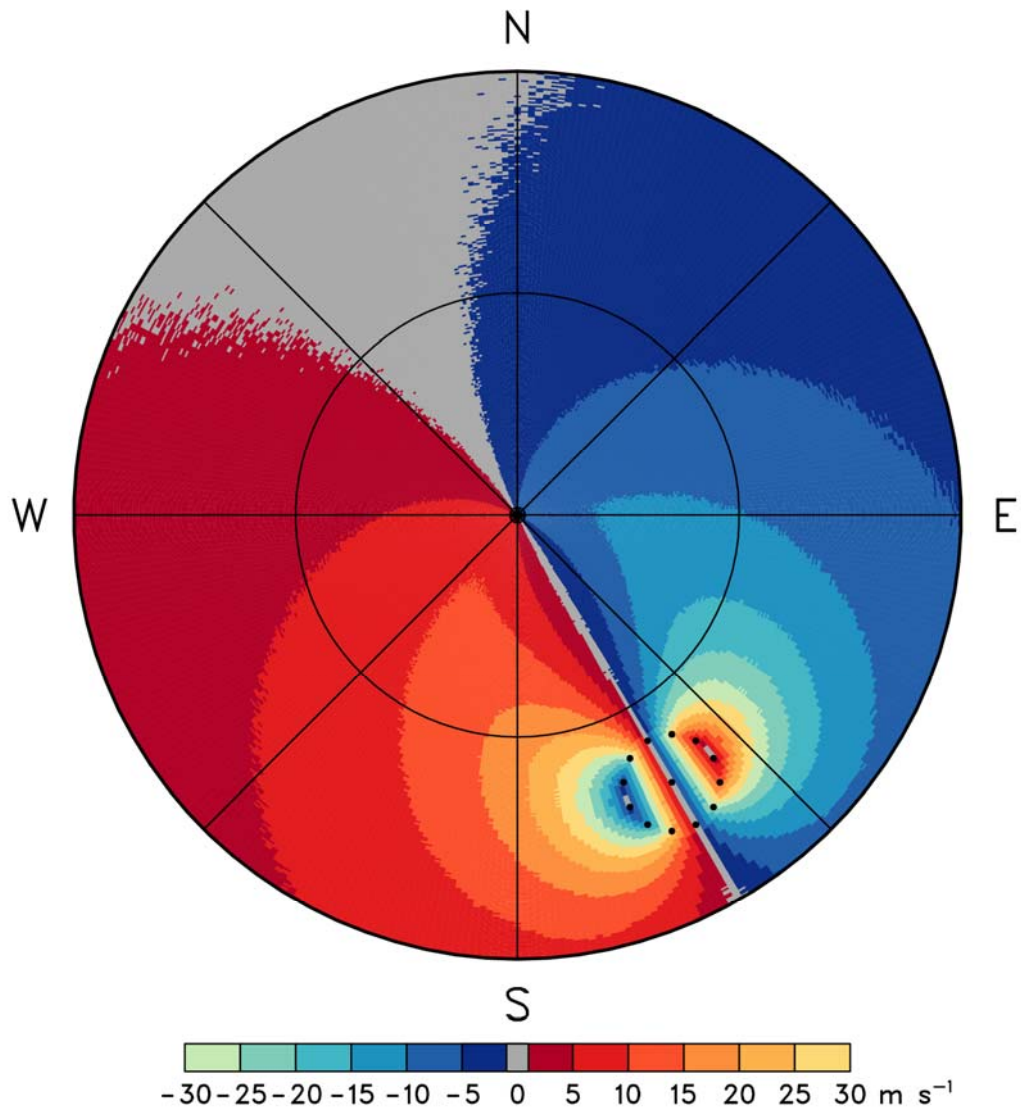


**Fig. 3.1.** Simulation of storm-relative Doppler velocities in a tropical cyclone at a range of 160 km (86 n mi) from a coastal Doppler radar (center of display). The two range circles are at distances of 115 (62) and 230 km (124 n mi) from the radar. The dotted circle surrounding the cyclone center (small dot) indicates the edge of the core region where the maximum winds are found.

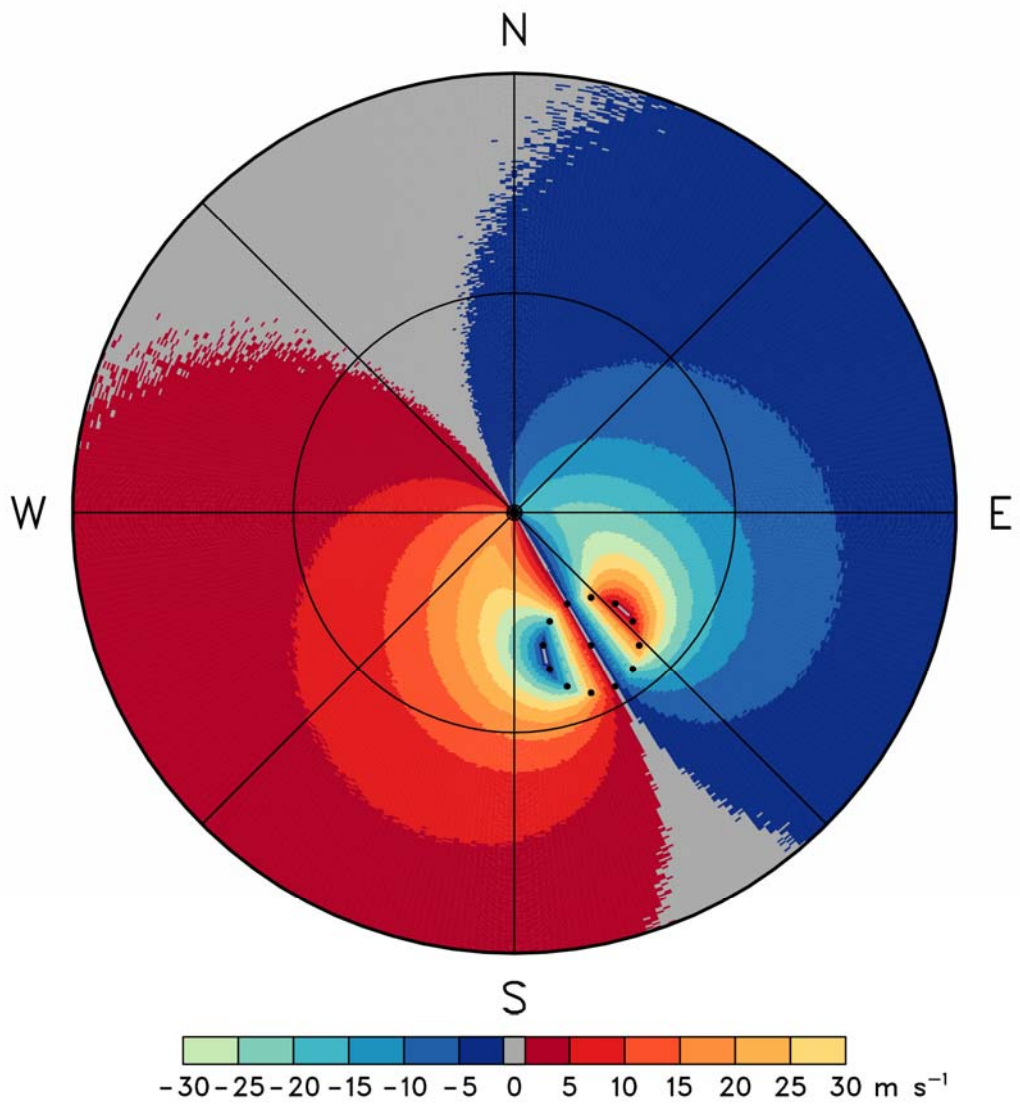


**Fig. 3.2.** Same as Fig. 3.1, except the tropical cyclone center is at a range of 80 km (43 n mi) from the radar. The overall Doppler velocity pattern is similar to that simulated by Baynton (1979).

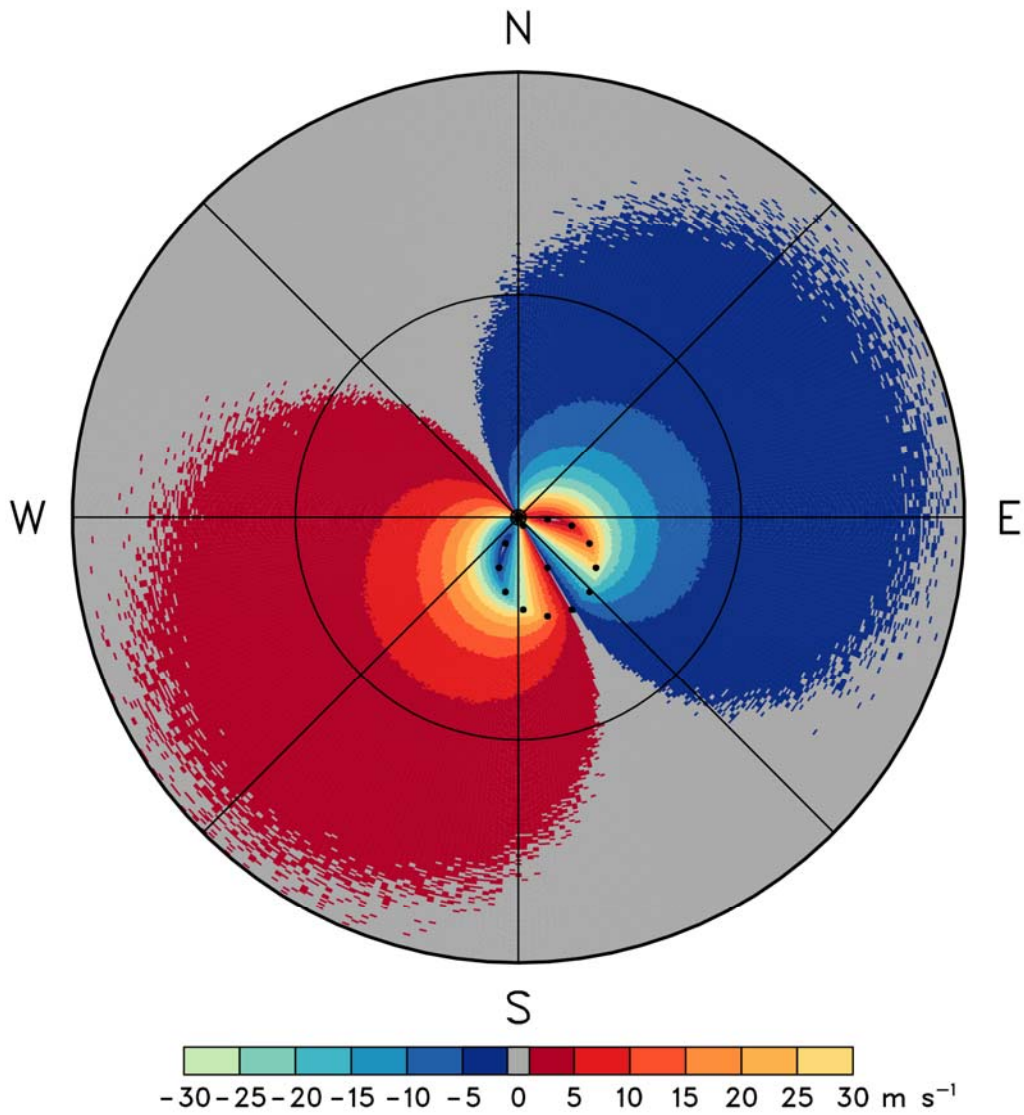


**Fig. 3.3.** Same as Fig. 3.1, except the tropical cyclone center is at a range of 30 km (16 n mi) from the radar. Note that the area of each Doppler velocity interval has been decreasing outside the core diameter (dotted circle), except for the near zero interval that has been increasing, as the tropical cyclone approaches the radar (Figs. 3.1 through 3.3). If an axisymmetric tropical cyclone were centered on the radar, all Doppler velocity values would be zero because the entire flow field would be perpendicular to all radial viewing directions.

## **4. INTERPRETATION OF DOPPLER VELOCITY PATTERNS WITHIN CONVECTIVE STORMS**

### **4.1 Introduction**

In this chapter, we display simulated flow fields and the corresponding Doppler velocity patterns within a 30 x 30 km (16 x 16 n mi) window located 100 km (54 n mi) due north of the radar. It is assumed that the Doppler radar scans horizontally through each flow field, which is a reasonable approximation given the small scale of the display. Except as noted, the simulated flow fields represent basic features without the addition of environmental winds and storm motion. Unlike the simulations in the previous chapters, no noise was added to the Doppler velocity data points. Since these Doppler velocity patterns are blown up, the blockiness associated with 250 m by 1.0° sampling becomes readily apparent.

A typical radar antenna produces a beam that is about 1.0° wide. Since the antenna typically scans horizontally while it collects a sufficient number of samples (minimum of about 30–50) to produce a representative mean Doppler velocity value, the beam is effectively broadened to about 1.5°. However, in order to clearly portray the essence of the patterns simulated in this chapter, the radar beam is assumed to have zero width. Consequently, we do not simulate the gradual degradation of convective-scale features that occurs when the linear width of the beam increases (constant angular width) as distance from the radar increases (e.g., Wood and Brown 1997).

With a beam of zero width, small-scale features like tornadoes are not degraded as they would be with a 1.5° effective beamwidth. Instead, we simulate tornadoes in Section 4.9 using the broader and weaker tornadic vortex signature (TVS) that would have resulted from sampling with a 1.5° effective beamwidth.

### **4.2 Patterns Associated with Constant Wind Speed and Direction**

In regions of a convective storm not directly affected by updrafts and downdrafts, the Doppler velocity pattern primarily reflects the relatively undisturbed environmental flow. It is difficult to deduce from the Doppler velocity pattern in Fig. 4.2.1 that the wind is blowing from the southwest at 25 m s<sup>-1</sup> (49 kt). About all one can tell is that the flow has a component away from the radar because the Doppler velocities in the window are positive.

The Doppler velocity pattern in Fig. 4.2.2 is somewhat easier to interpret. When the radar points due north, the Doppler velocity value is zero. Negative velocities to the left of the zero band indicate a component of the wind toward the radar and positive values to the right indicate a component away from the radar. We can state with confidence, then, that the wind is blowing from the west, but we are unable to determine the wind speed. For the situations shown in Figs. 4.2.1 and 4.2.2, we would have been able to determine both wind speed and direction if we were able to see the entire PPI display, as in the figures shown in Chapter 2.

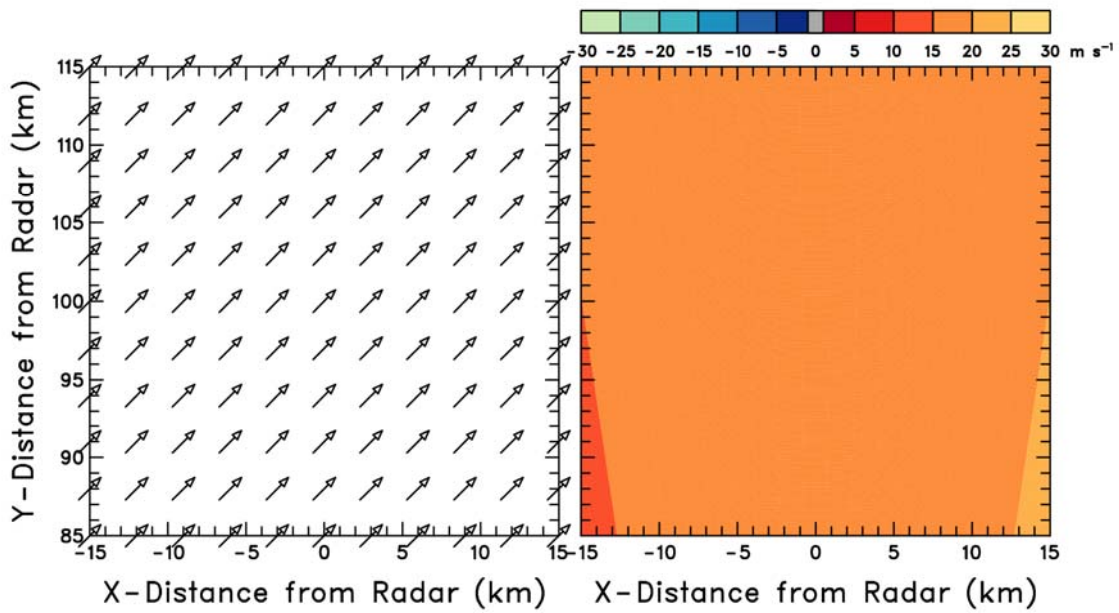


*Fig. 4.2.1. Doppler velocity pattern (right) corresponding to a uniform horizontal wind blowing from the southwest toward the northeast at a speed of  $25 \text{ m s}^{-1}$  (49 kt) (left). Positive Doppler velocities represent flow away from the radar, which is located 100 km (54 n mi) south of the display center.*

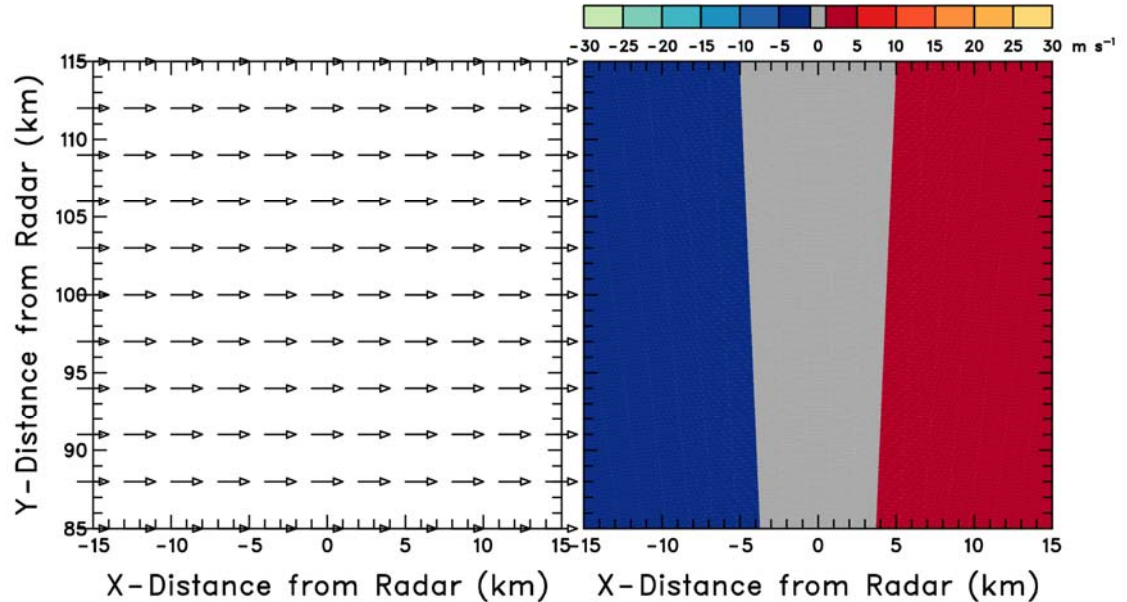


*Fig. 4.2.2. Same as Fig. 4.2.1, except the wind is blowing from the west at a speed of  $25 \text{ m s}^{-1}$  (49 kt). Negative (positive) Doppler velocities represent flow toward (away from) the radar.*

### 4.3 Patterns Associated with Axisymmetric Vortices

Axisymmetric flow around a vertical axis can be approximated by the overly simplified Rankine combined velocity profile, as discussed in the previous chapter. An anticyclonic (clockwise) circulation (mesoanticyclone) is simulated in Fig. 4.3.1. The zero Doppler velocity band lies along the radial direction from the radar through the circulation center because flow at all ranges is perpendicular to that viewing direction. (If the radar beam were not directed exactly toward the circulation center, but slightly offset, the positive and negative values would be adjacent to each other with no intervening zero band.) The negative Doppler velocity extreme on the right represents peak tangential velocity toward the radar at the core radius. The positive Doppler velocity extreme on the left, also at the core radius, represents peak tangential velocity away from the radar. Mesoanticyclones often are found in the left-moving members of splitting severe storms.

A cyclonic circulation representing a thunderstorm mesocyclone is simulated in Fig. 4.3.2. The circulation, as well as the Doppler velocity pattern, is a mirror image of the anticyclonic case. If the mesocyclone were moving toward the north at  $18 \text{ m s}^{-1}$  (35 kt), Fig. 4.3.3 indicates that the flow field and colors (representing Doppler velocity values) are different but that the overall Doppler velocity *pattern* within and surrounding the core region remains basically the same. In practice, a Doppler velocity display will look more like Fig. 4.3.3 than Fig. 4.3.2 because there typically will be a Doppler component of mesocyclone/storm motion present. When the estimated mesocyclone/storm component of motion is subtracted from the Doppler velocity display, the resulting pattern (representing storm-relative flow) becomes more balanced (as in Fig. 4.3.2).

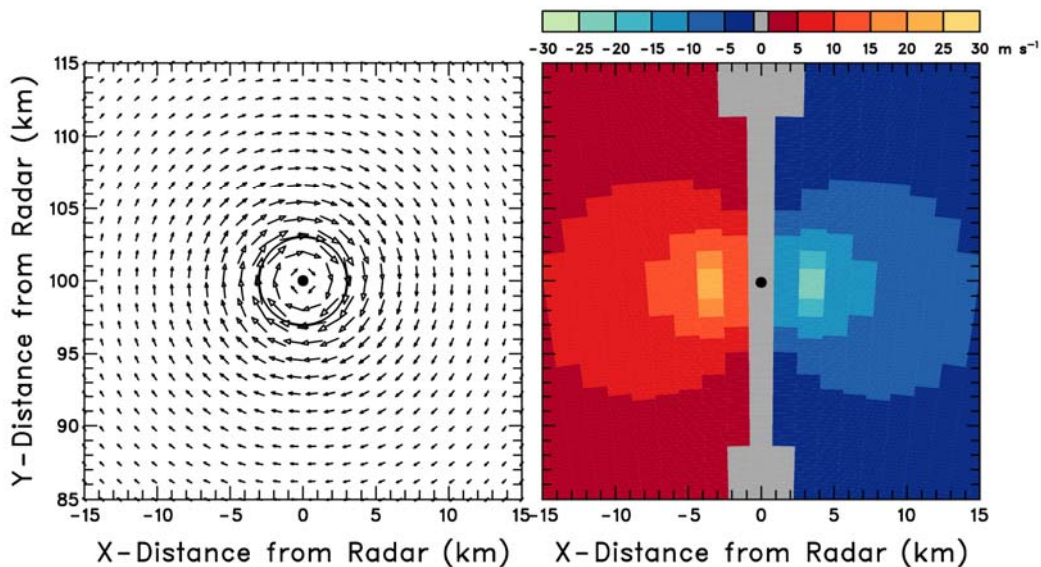


**Fig. 4.3.1.** Doppler velocity pattern (right) of a mesoanticyclone (left) that has peak tangential velocities of  $25 \text{ m s}^{-1}$  (49 kt) at a radius of 3 km (1.6 n mi) from the circulation center (black dot); radius of maximum winds is indicated by circle. Arrow length is proportional to wind speed.

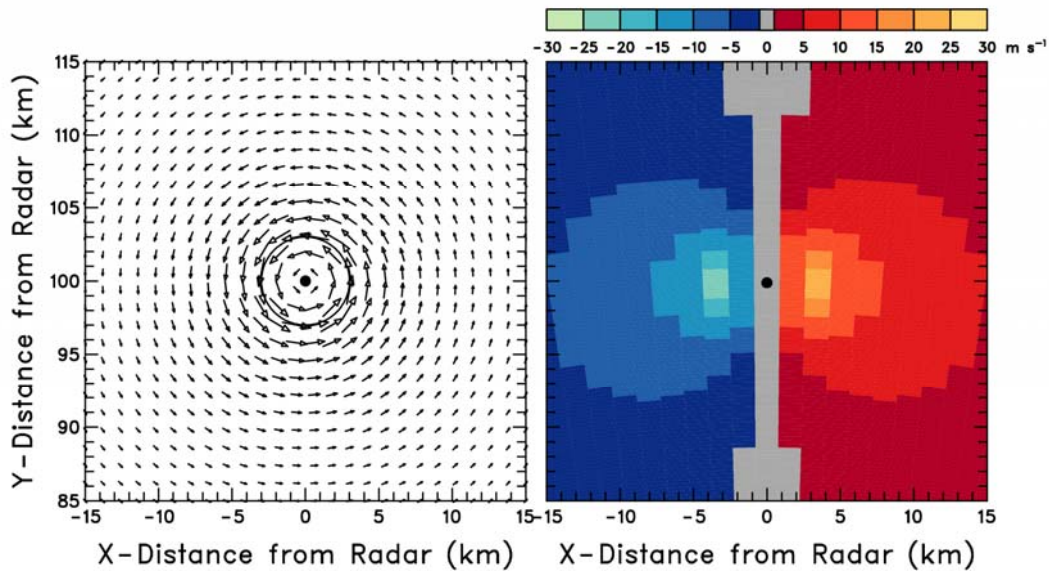


**Fig. 4.3.2.** Same as Fig. 4.3.1, except that the Doppler velocity pattern (right) corresponds to a mesocyclonic (left) that has peak tangential velocities of  $25 \text{ m s}^{-1}$  (49 kt) at a radius of 3 km (1.6 n mi) from the circulation center (black dot).

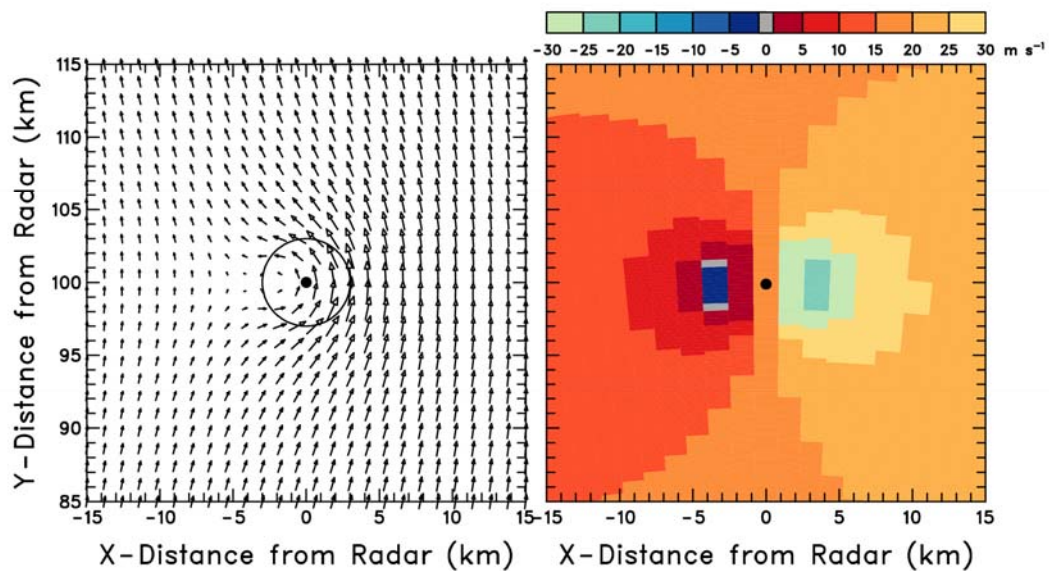


**Fig. 4.3.3.** Same as Fig. 4.3.2, except that the mesocyclone is moving toward the north at  $18 \text{ m s}^{-1}$  (35 kt). Though the Doppler velocity pattern (right) remains essentially unchanged, the apparent circulation center in the flow field (left) is displaced to the left of the true circulation center. Note that Doppler velocity values exceeding  $30 \text{ m s}^{-1}$  on the right side of the circulation are aliased.

#### 4.4 Patterns Associated with Axisymmetric Radial Flow

A Rankine combined velocity profile also can be used to simulate axisymmetric convergent and divergent flow. In this case, the core radius is the radius at which the inflow or outflow wind speed is a maximum. An example of simulated convergent flow is shown in Fig. 4.4.1. The zero band indicates the portion of the wind field that is perpendicular to the radar viewing direction. At infinite distance from the radar, the zero velocity band would be a straight line. However, at finite distances, the zero band is curved with the radar on the concave side (e.g., Wood and Brown 1992). Convergent flow is toward the radar on the far side of the zero band and away from the radar on the near side. The two regions with extreme Doppler velocities are located at distances from the convergence center equal to the core radius.

The divergence pattern in Fig. 4.4.2 is analogous to the convergence pattern but with the colors—and flow directions—reversed. It represents divergence that is found within the upper portions of an updraft or within a microburst beneath a downdraft at the earth's surface. When the feature is moving toward the north at  $18 \text{ m s}^{-1}$  (35 kt) or has a uniform flow field of  $18 \text{ m s}^{-1}$  from the south superimposed on it (Fig. 4.4.3), the divergent flow pattern becomes distinctly different with the apparent divergence center displaced to the south; the true divergence center is indicated by the black dot. Also, the Doppler velocities are distinctly different, with only a small region of negative velocities and a larger region of aliased positive velocities. However, comparison of Figs. 4.4.2 and 4.4.3 reveals that the overall Doppler velocity *pattern* within and surrounding the core region remains essentially unchanged with the addition of a uniform motion/flow field.

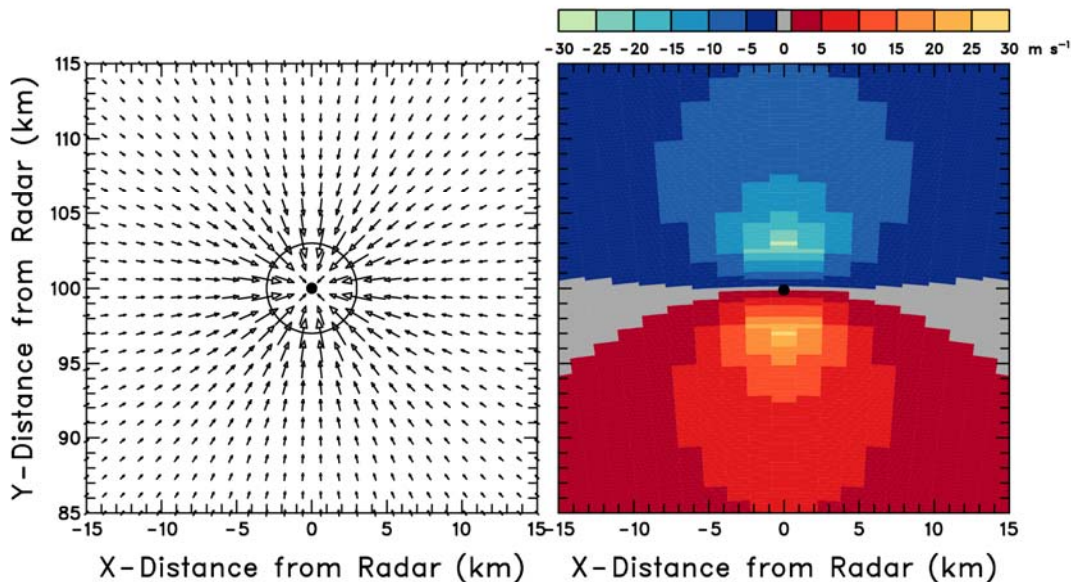


**Fig. 4.4.1.** Doppler velocity pattern (right) corresponding to axisymmetric convergent flow (left). The maximum radial velocity of  $25 \text{ m s}^{-1}$  (49 kt) is at a core radius of 3 km (1.6 n mi); the radius of maximum winds is indicated by the circle. Black dot represents the center of the flow. Arrow length is proportional to wind speed. Negative (positive) Doppler velocities represent flow toward (away from) the radar.

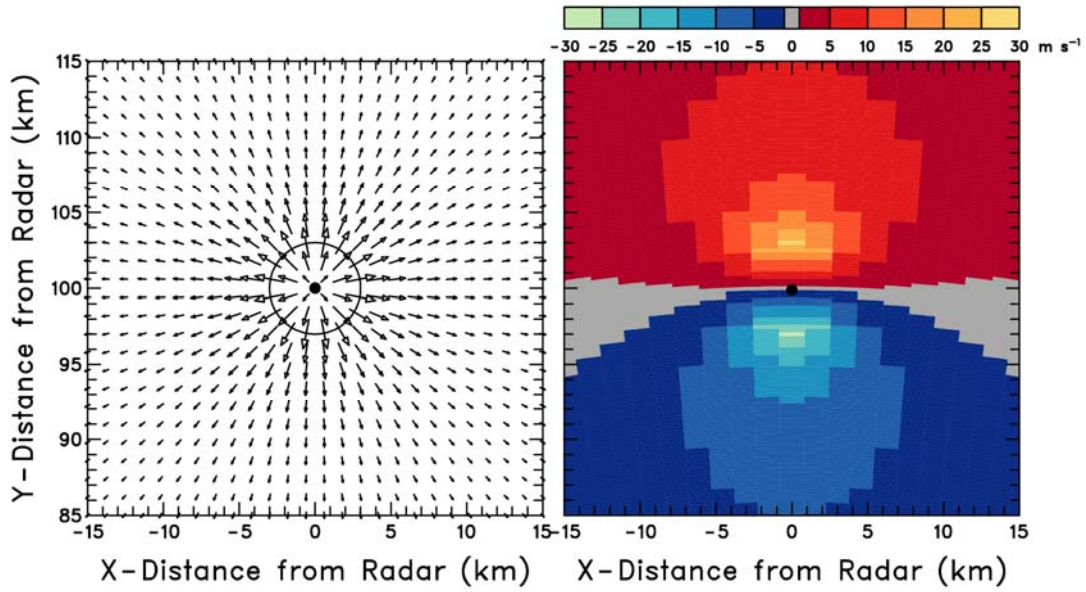


**Fig. 4.4.2.** Same as Fig. 4.4.1, except that the Doppler velocity pattern (right) corresponds to axisymmetric divergent flow (left).

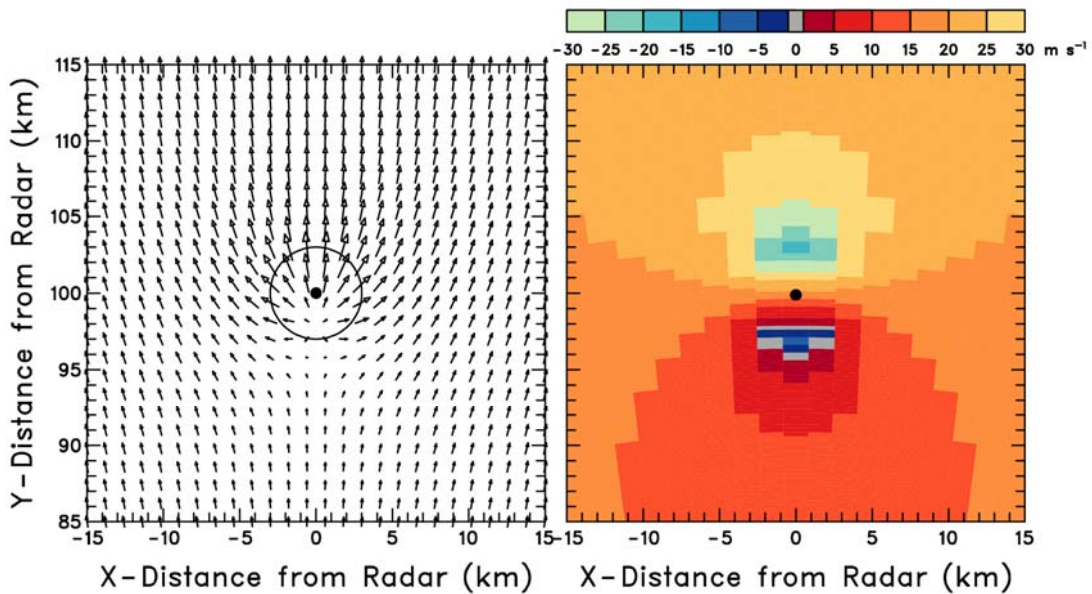


**Fig. 4.4.3.** Same as Fig. 4.4.2, except that the divergence feature is moving to the north at  $18 \text{ m s}^{-1}$  (35 kt) or a uniform flow field of  $18 \text{ m s}^{-1}$  from the south is superimposed on it. Note that Doppler velocity values exceeding  $30 \text{ m s}^{-1}$  on the far side of the divergence center are aliased.

## 4.5 Mesocyclone and Divergence Patterns Viewed from Four Different Directions

It is frequently necessary for weather decision makers to view storm features using multiple radars. Knowing each radar's location relative to a particular feature is critical for proper signature recognition. For example, the Doppler velocity patterns representing mesocyclonic and divergent flows in Sections 4.3 and 4.4 are nearly the same except for a rotational difference of 90°. Thus, in order to distinguish between rotation and divergence, it is vital that the pattern be interpreted relative to the viewing direction from the radar.

Figures 4.5.1 and 4.5.2 are presented in order to emphasize the importance of the viewing direction. In all cases, the display window is oriented with north toward the top. In Fig. 4.5.1, when a radar scans past a mesocyclone, flow away from the radar always is on the right and flow toward the radar always is on the left *relative to the radar viewing direction*. In Fig. 4.5.2, when a radar scans past a divergence region, flow toward the radar always is on the near side and flow away from the radar always is on the far side.

The mesocyclone pattern to the south of the radar (Fig. 4.5.1), for example, is similar to the divergence pattern to the west of the radar (Fig. 4.5.2). Without knowing the location of the radar relative to the window, it is not possible to properly interpret the type of flow field that produced the Doppler velocity pattern.

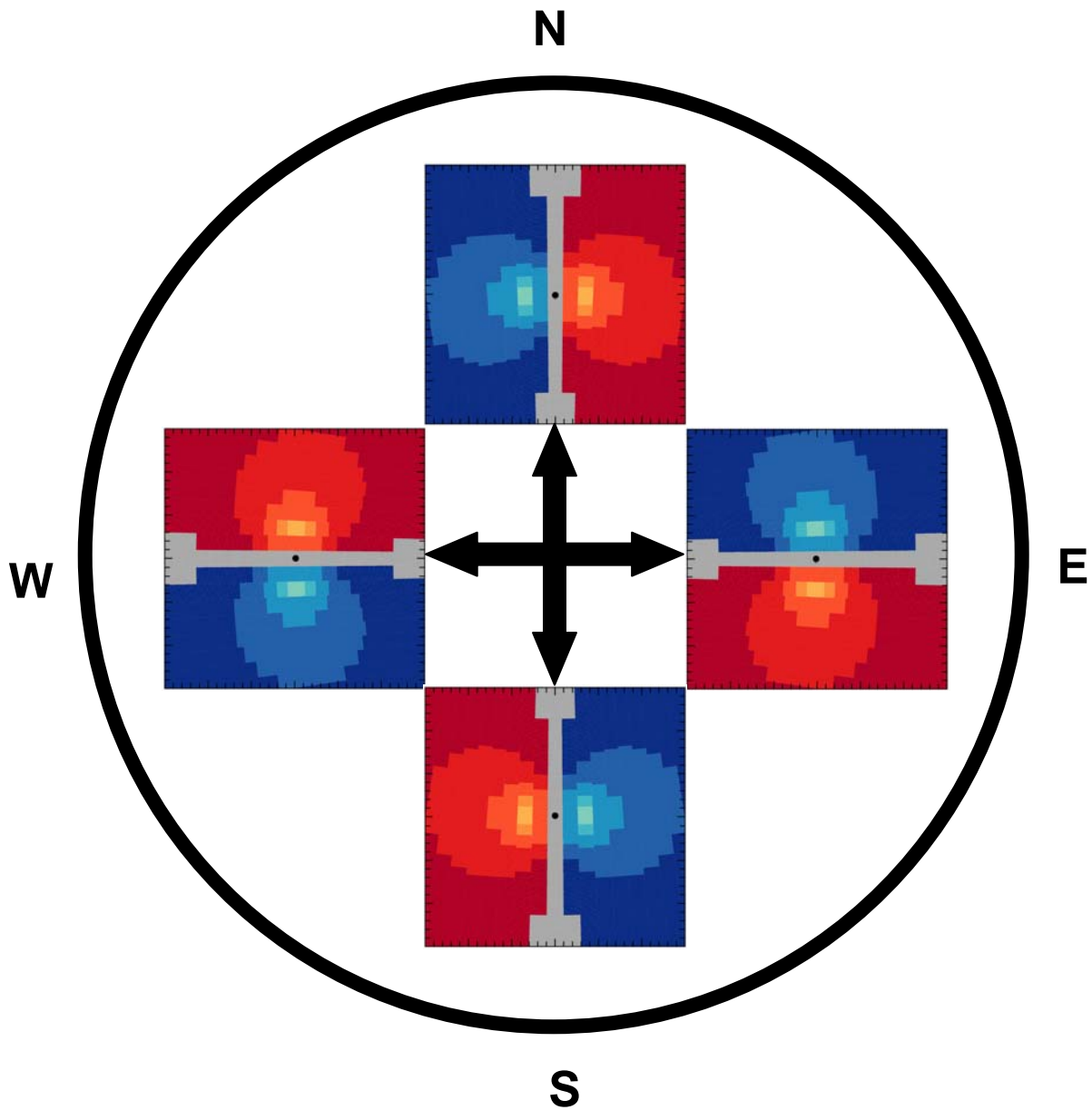


*Fig. 4.5.1. Doppler velocity patterns for a mesocyclone viewed by a radar (located at the center) from four different directions.*

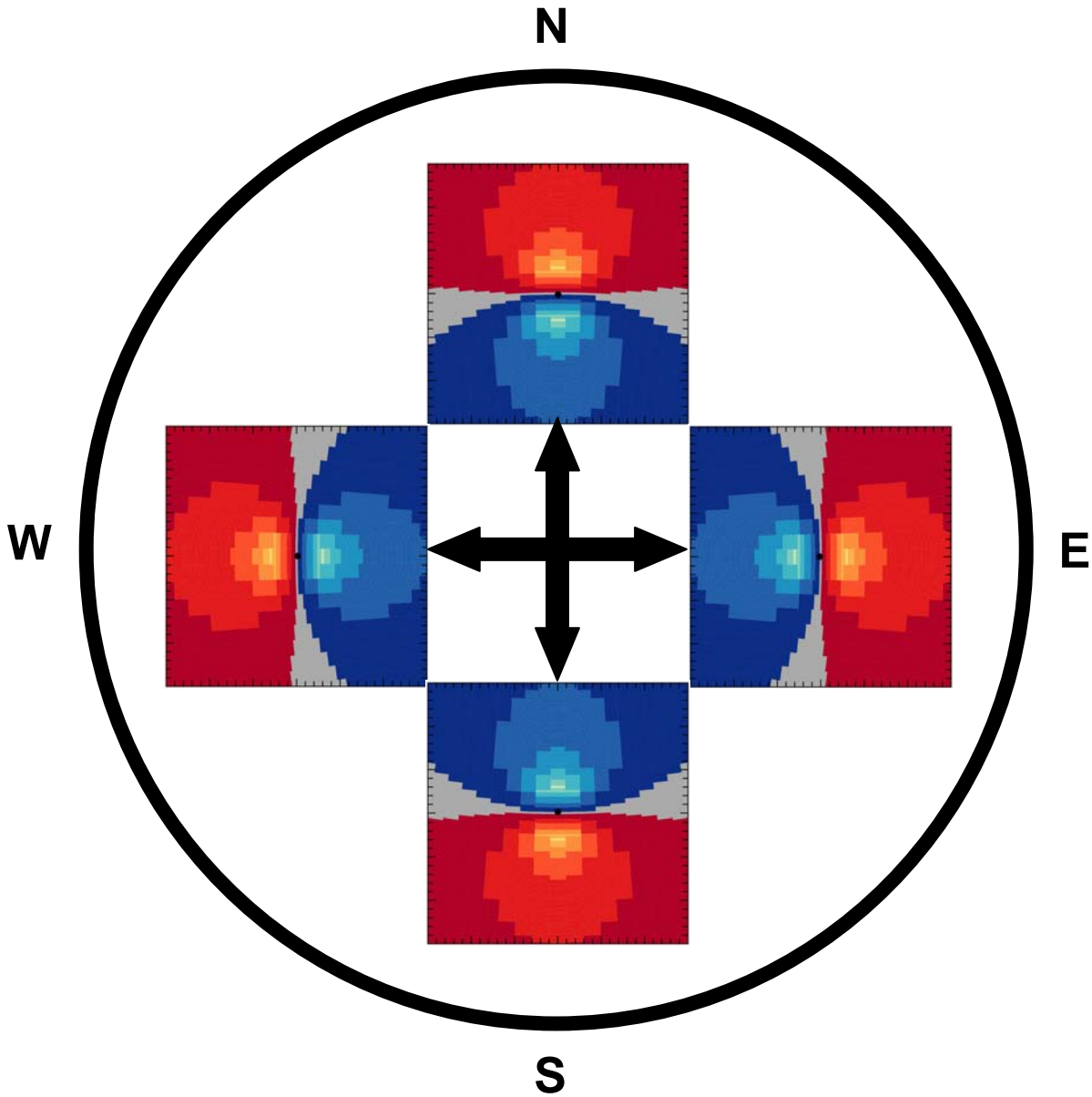


*Fig. 4.5.2. Doppler velocity patterns for axisymmetric divergence viewed by a radar (located at the center) from four different directions.*

## 4.6 Distortion of Doppler Velocity Patterns Owing to Proximity to the Radar

For the mesocyclone and divergence Doppler velocity patterns discussed in Sections 4.3 through 4.5, the radar was located 100 km (54 n mi) from the center of the flow features. When the radar is closer to the features, the patterns become more distorted like those for the tropical cyclone discussed in Chapter 3.

In Fig. 4.6.1, the radar is only 10 km (5 n mi) south of the mesocyclone center. The weaker Doppler velocities associated with the signature extend southward and converge at the radar position. The boundaries between colors on the inside of the mesocyclone's core region are along imaginary lines radiating out from the radar location; this feature is not as obvious with vortices that have assumed profiles different from a Rankine profile.

At a range of 30 km (16 n mi), the mesocyclone signature is less distorted (Fig. 4.6.2). The Doppler velocity areas outside the mesocyclone's core region extend southward to some extent toward the radar.

The zero Doppler velocity band for axisymmetric convergence located 10 km from the radar (right part of Fig. 4.6.3) has a unique shape—the center of the zero band is a circle passing through the radar and the convergence center. Note that the chord connecting the two points is the diameter of the circle. From plane geometry we know that any angle inscribed in a semicircle is a right angle. Therefore, at that point along the radar viewing direction where the radial line intersects the zero line, the radial line is perpendicular to the convergent (or divergent) streamline flowing straight into (out of) the center of the convergence (divergence) signature.

At a range of 30 km (Fig. 4.6.4), the zero Doppler velocity band is less curved because the center of the band now is part of a circle whose diameter is 30 km. Consequently, the extreme positive and negative Doppler velocity regions are more nearly symmetric.

At a range of 100 km (54 n mi), the distorted character of the mesocyclone (Fig. 4.3.2) and convergence (Fig. 4.4.1) patterns is less noticeable. However, one may note that there is evidence that the color boundaries within the mesocyclone core region are oriented along imaginary lines radiating from the radar. For the convergence pattern, there is a suggestion that the center of the zero band is part of a circle 100 km in diameter.

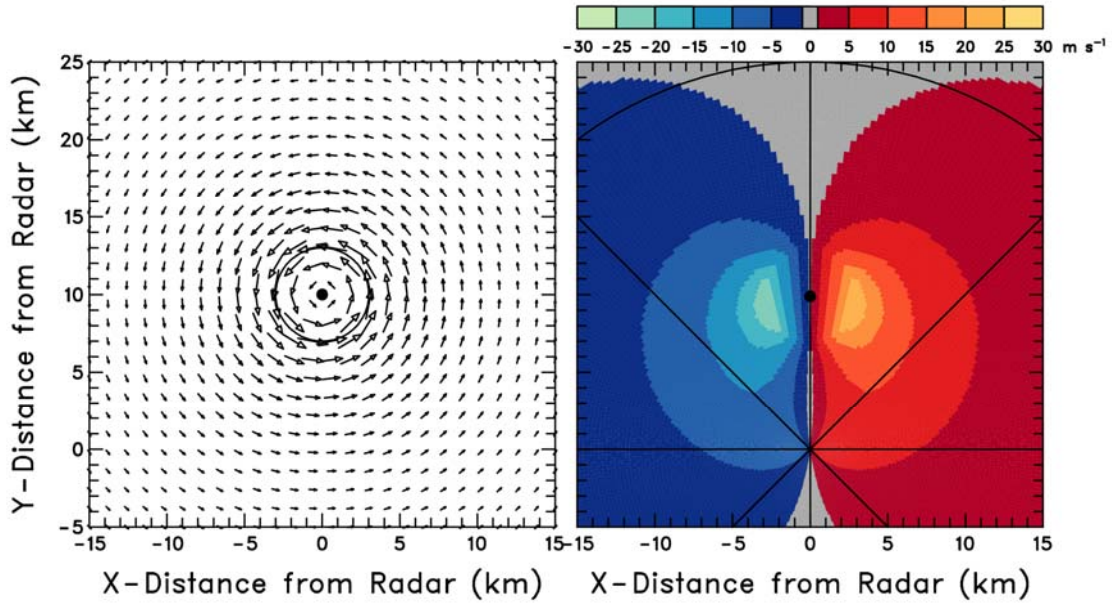


**Fig. 4.6.1.** Doppler velocity pattern of a mesocyclone when the center (dot at center of window) is located 10 km (5 n mi) north of the radar; the radar is located at the point where radial lines intersect near bottom center of the window. Core radius is 3 km (1.6 n mi) and peak velocity is  $25 \text{ m s}^{-1}$  (49 kt). Negative (positive) Doppler velocities represent flow toward (away from) the radar.

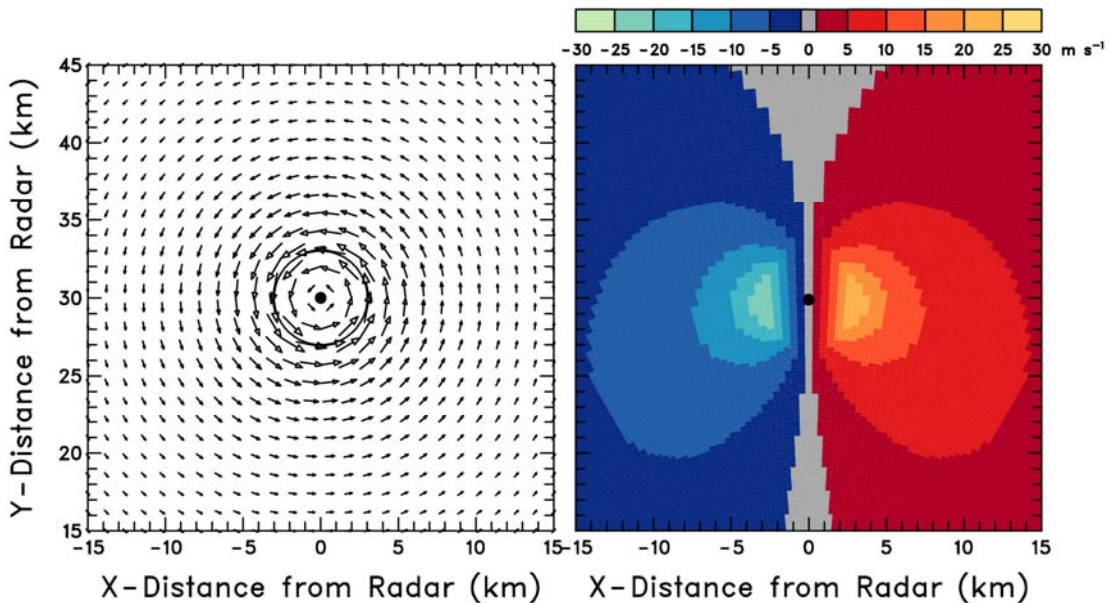


**Fig. 4.6.2.** Same as Fig. 4.6.1, except that the center of the mesocyclone is 30 km (16 n mi) north of the radar.

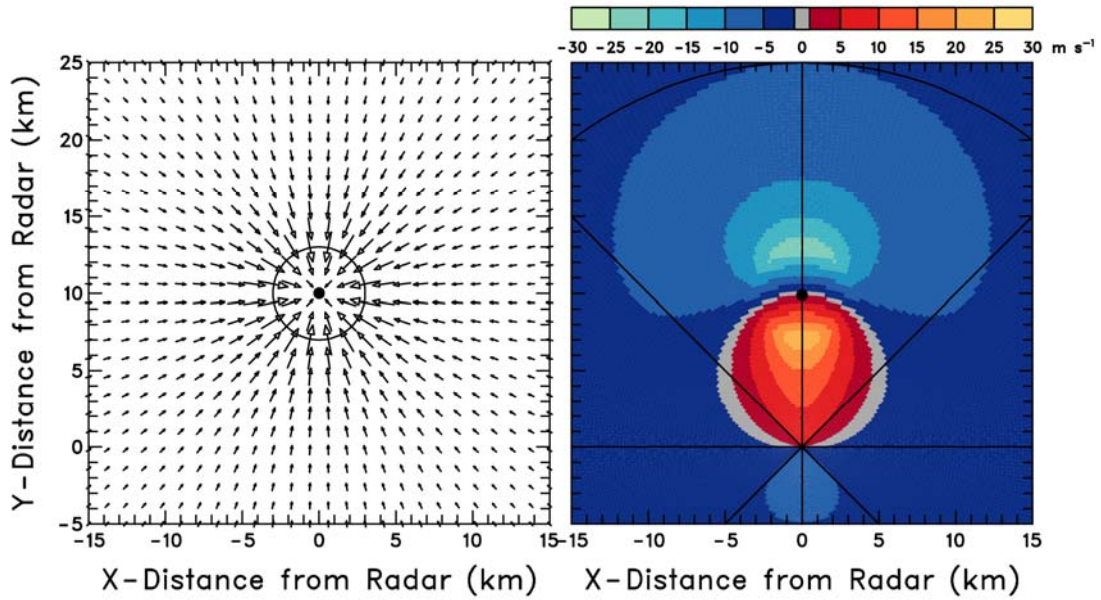


**Fig. 4.6.3.** Doppler velocity pattern of axisymmetric convergence when the center is located 10 km (5 n mi) north of the radar; the radar is located at the point where radial lines intersect near bottom center of the window. Core radius is 3 km (1.6 n mi) and peak velocity is  $25 \text{ m s}^{-1}$  (49 kt).

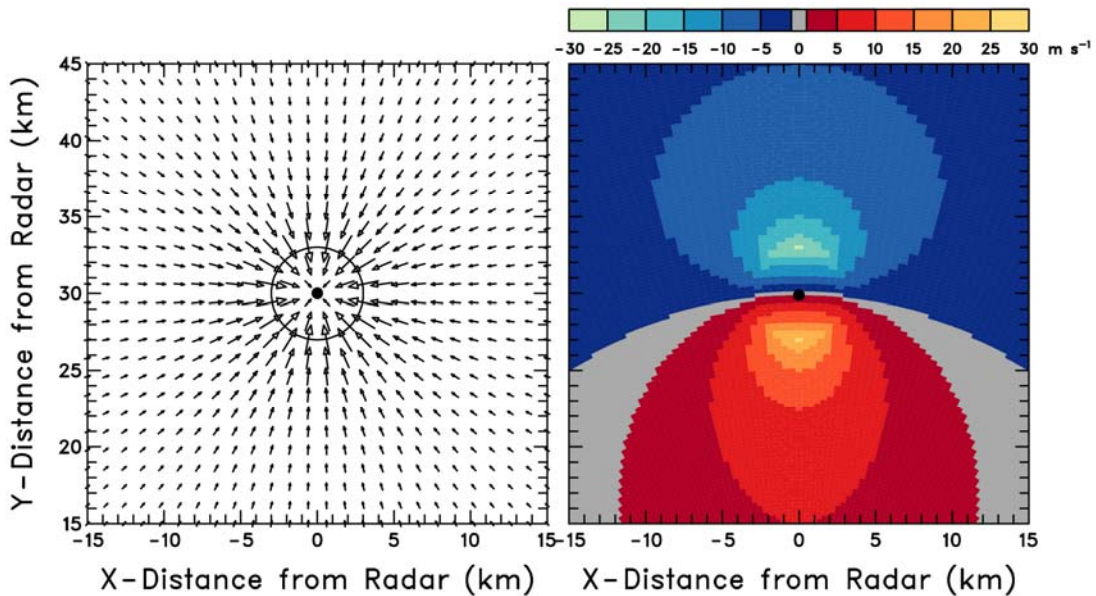


**Fig. 4.6.4.** Same as Fig. 4.6.3, except that the convergence center is 30 km (16 n mi) north of the radar.

## 4.7 Patterns Associated with a Convergent/Divergent Mesocyclone

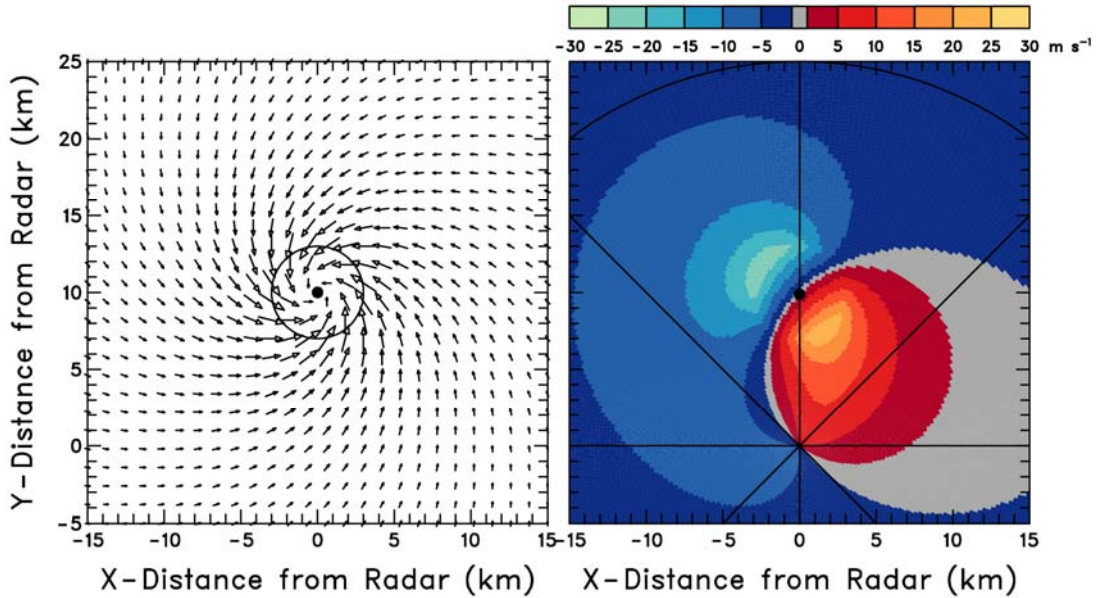
When the rotation and convergence/divergence fields of Sections 4.3, 4.4, and 4.6 are combined and have the same core radius, the resulting Doppler velocity pattern resembles a Rankine combined velocity profile. The primary distinction is that the zero band is neither parallel nor perpendicular to the radar viewing direction. Instead, the zero band is at an intermediate angle depending on the relative peak velocities of the two flow field components. If both the peak velocities and core radii are different, the resulting Doppler velocity pattern is more complicated.

Figure 4.7.1 shows the combination of convergence and cyclonic rotation where the core radii are the same and the peak velocities are the same; the feature center is 10 km (5 n mi) north of the radar. In this case, the pattern is rotated  $45^\circ$ , midway between the Doppler velocity patterns for cyclonic rotation and convergence (see Figs. 4.6.1 and 4.6.3). The center of the zero Doppler velocity band is a circle that passes through the radar and the center of the flow feature, but the diameter of the circle no longer passes through both points.

At a greater range of 30 km (16 n mi), the pattern in Fig. 4.7.2 is midway between the cyclonic rotation and convergence patterns in Figs. 4.6.2 and 4.6.4. The same is true for the pattern at 100 km (54 n mi) distance in Fig. 4.7.3 (compare with Figs. 4.3.2 and 4.4.1).

The combination of divergence and cyclonic rotation in Fig. 4.7.4 is midway between that for divergence (Fig. 4.4.2) and for cyclonic rotation (Fig. 4.3.2). Combinations of anticyclonic rotation with convergence and with divergence having the same core radii and peak velocities produce similarly rotated patterns that are midway between the respective individual Doppler velocity patterns.

When the convergence/divergence and rotation fields are not of the same size and strength, curious Doppler velocity patterns are produced. Figure 4.7.5 shows the results of combining stronger and smaller cyclonic rotation with weaker and larger convergence. The reverse is shown in Fig. 4.7.6. In both situations, the overall orientation of the zero Doppler velocity band indicates a combination of convergence and cyclonic rotation (as in Fig. 4.7.3). The clue in Fig. 4.7.5 that the stronger field is rotation is that the pattern of extreme Doppler velocity values at the center of the pattern is only slightly rotated from a pure rotation pattern. Analogously, the central pattern of extreme Doppler velocity values in Fig. 4.7.6 is only slightly rotated from a pure convergence pattern.



**Fig. 4.7.1.** Doppler velocity pattern (right) corresponding to combination of convergence and cyclonic rotation fields (left) having the same core radius (3 km or 1.6 n mi); maximum inflow velocity and maximum rotational velocity are the same with maximum resultant velocity being  $25 \text{ m s}^{-1}$  (49 kt). Black dot represents the feature center and the circle indicates radius of maximum winds. Arrow length is proportional to wind speed. The feature center is 10 km (5 n mi) due north of the radar. Negative (positive) Doppler velocities represent flow toward (away from) the radar.

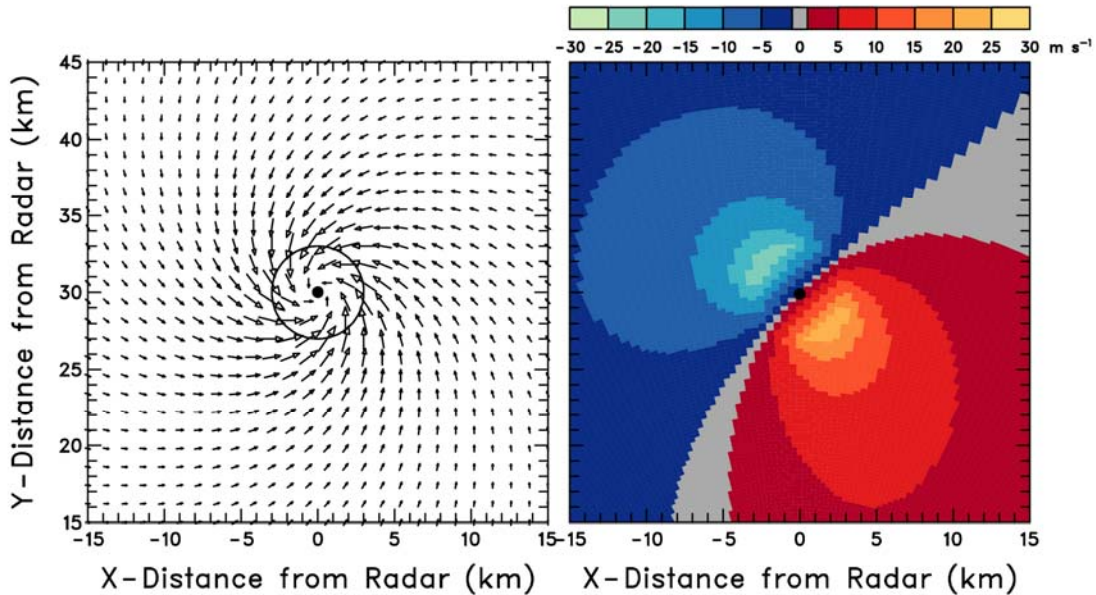


**Fig. 4.7.2.** Same as Fig. 4.7.1, except that feature center is 30 km (16 n mi) due north of the radar.

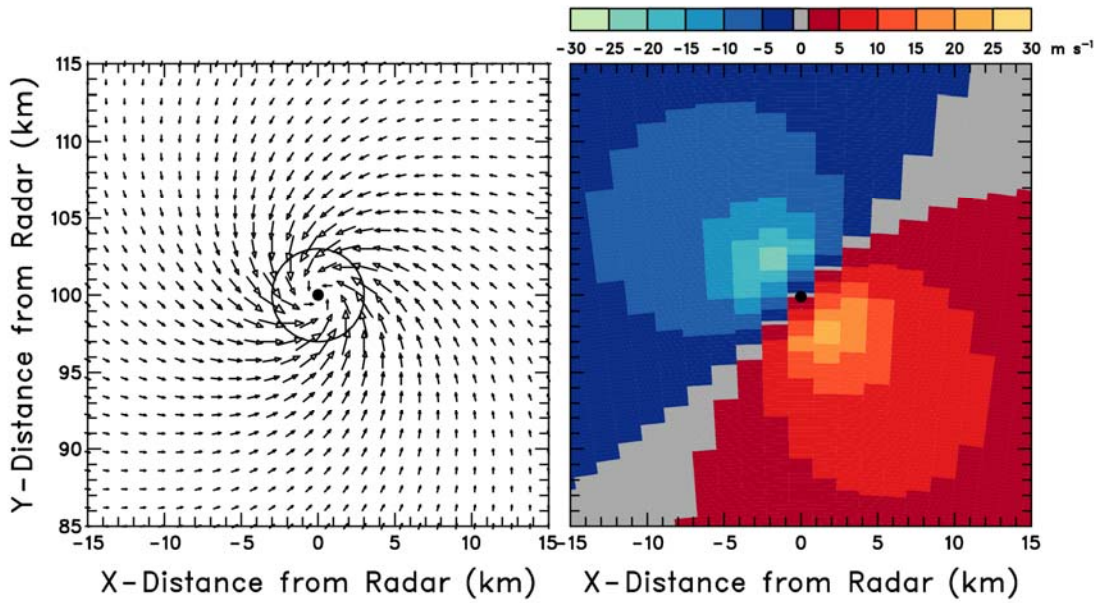


**Fig. 4.7.3.** Same as Fig. 4.7.1 (convergence and cyclonic rotation), except that the feature center is 100 km (54 n mi) due north of the radar.

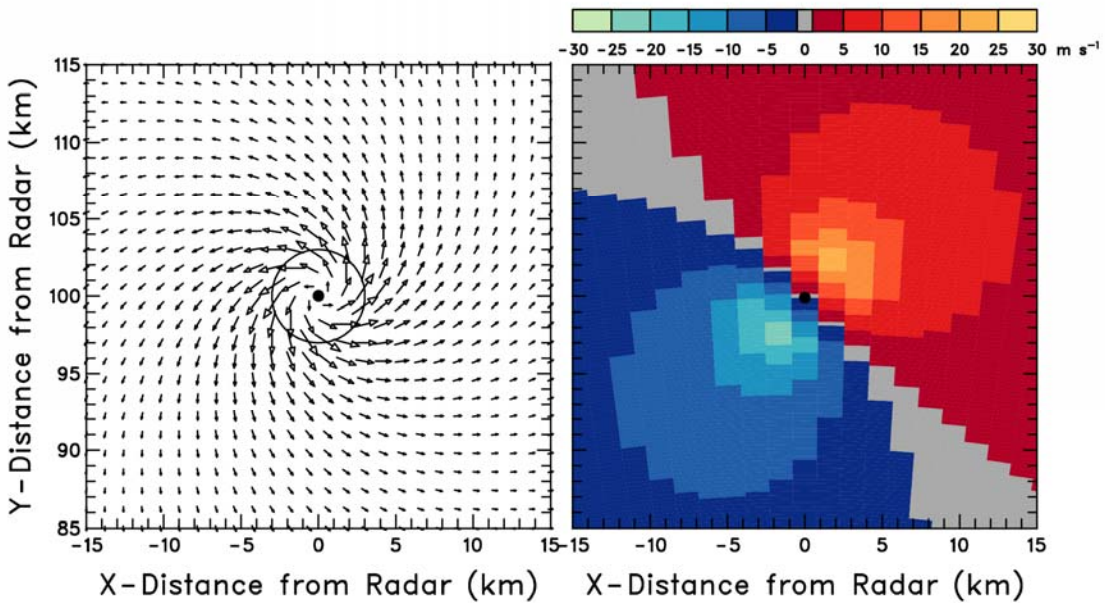


**Fig. 4.7.4.** Same as Fig. 4.7.3, except that the flow field is a combination of divergence and cyclonic rotation.

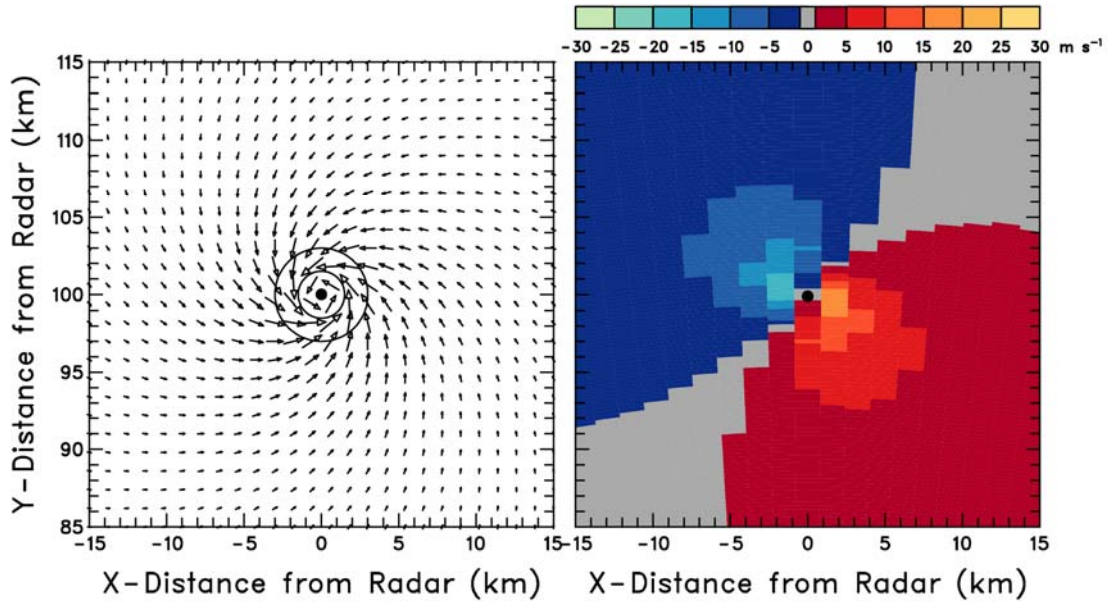


**Fig. 4.7.5.** Doppler velocity pattern (right) corresponding to cyclonic rotation that is stronger and smaller (peak tangential velocity is  $20 \text{ m s}^{-1}$  or 39 kt, core radius is 1.5 km or 0.8 n mi) than axisymmetric convergence (peak radial velocity is  $10 \text{ m s}^{-1}$  or 19 kt, core radius is 3 km or 1.6 n mi). The feature center is 100 km (54 n mi) due north of the radar.

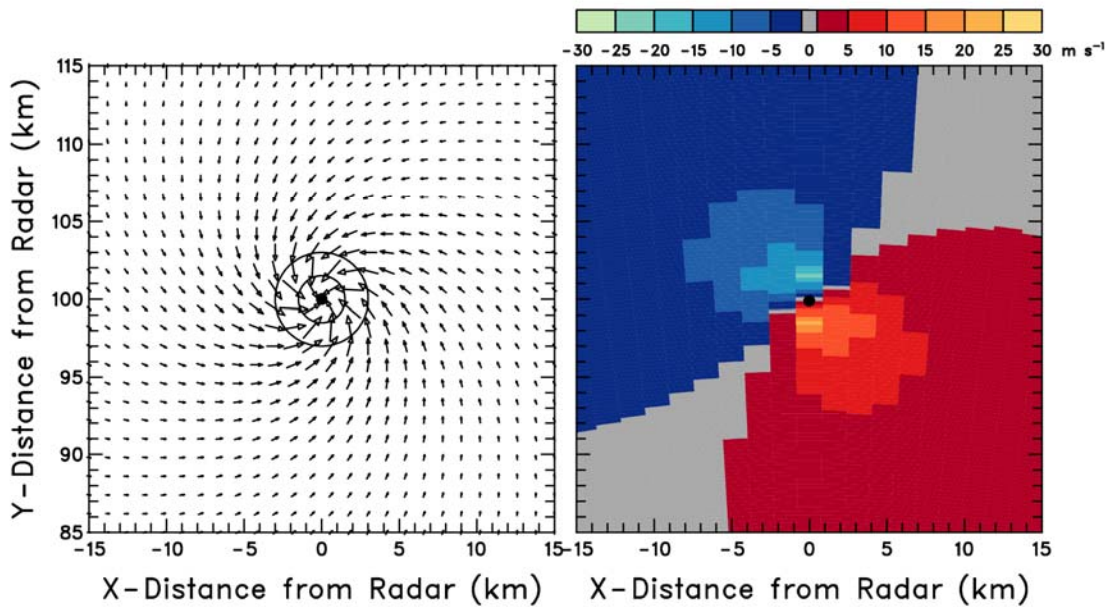


**Fig. 4.7.6.** Similar to Fig. 4.7.5, except that the convergence is stronger and smaller (peak radial velocity is  $20 \text{ m s}^{-1}$  or 39 kt, core radius is 1.5 km or 0.8 n mi) than cyclonic rotation (peak tangential velocity is  $10 \text{ m s}^{-1}$  or 19 kt, core radius is 3 km or 1.6 n mi).

#### **4.8 Patterns Associated with Two Mesocyclones having the Same Size and Strength**

Mesocyclones associated with supercell thunderstorms undergo a periodic evolution at roughly 45-minute intervals, where the mesocyclone core region weakens and a new core region concurrently forms on its right flank (e.g., Burgess et al. 1982). This phenomenon is simulated at a height of about 5 km (16 kft) in Figs. 4.8.1 and 4.8.2. The centers of the two core regions are separated by a distance equal to three core radii.

In Fig. 4.8.1, the radar viewing direction is normal to an imaginary line connecting the circulation centers. The magnitudes of the peak Doppler velocities of each mesocyclone core region are decreased between the two centers owing to the opposing flow induced by the other core region. On the other hand, the magnitudes of the peak Doppler velocities on the outer portions of each core region are increased owing to flow in the same direction from both circulations. At first glance, one might mistaken the pattern to be one for a single mesocyclone.

When the radar viewing direction is at a  $45^\circ$  angle to an imaginary line connecting the circulation centers (Fig. 4.8.2), the two circulations are offset enough for the signatures of two separate mesocyclones to be more apparent. One might erroneously deduce the presence of convergence at the center of the window; however, this feature is simply deformation arising from the juxtaposition of the two rotational fields viewed at this angle (see left side of Fig. 4.8.2). Note that the prevailing orientation of the zero band indicates the overall presence of cyclonic rotation.

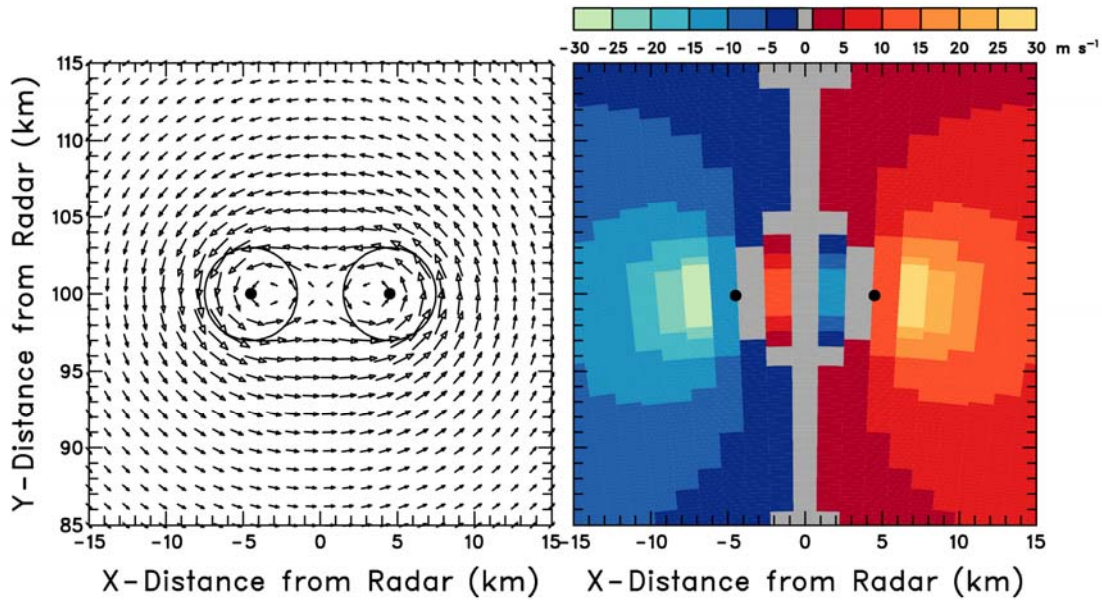


**Fig. 4.8.1.** Doppler velocity pattern (right) corresponding to two identical mesocyclones (peak tangential velocity is  $25 \text{ m s}^{-1}$  or 49 kt, core radius is 3 km or 1.6 n mi) whose centers are three core radii apart (left). Black dots represent the mesocyclone centers. Arrow length is proportional to wind speed. Negative (positive) Doppler velocities represent flow toward (away from) the radar.

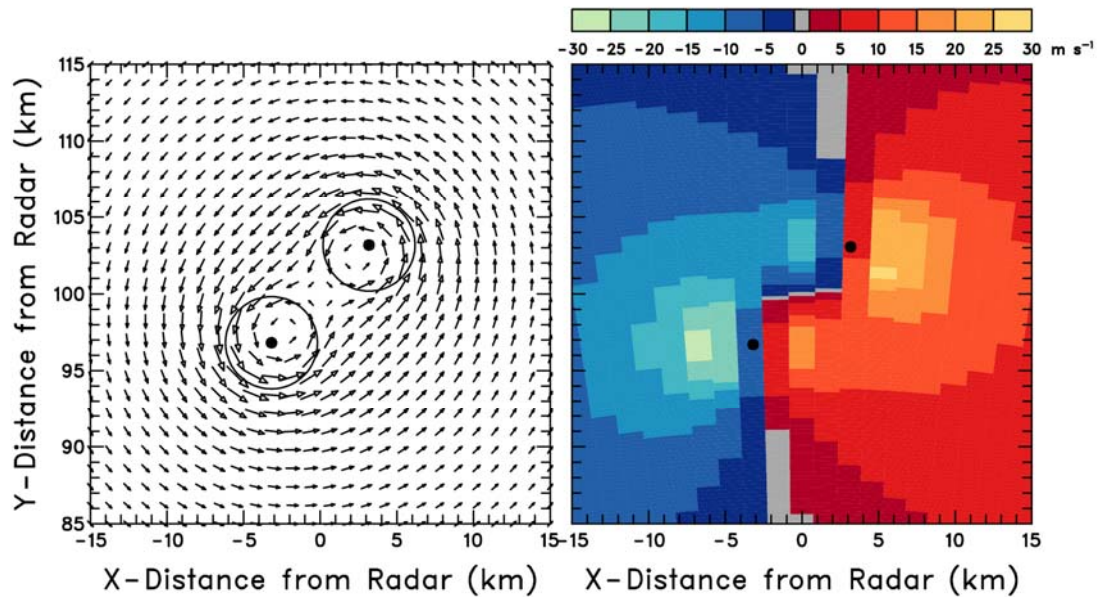


**Fig. 4.8.2.** Same as Fig. 4.8.1, except that an imaginary line through the mesocyclone centers is oriented  $45^\circ$  to the radar viewing direction.

#### 4.9 Patterns Associated with a Tornadic Vortex Signature within the Parent Mesocyclone

Nearly all significant tornadoes form within a pre-existing parent mesocyclone and typically are found within the mesocyclone's core region. Since all but the largest and closest tornadoes are smaller than the radar's beamwidth, the tornado's tangential velocities are greatly smoothed (degraded) within the radar beam. Consequently, the Doppler velocities within the resulting tornadic vortex signature (TVS) do not reflect either the size or strength of the tornado but rather some indeterminable combination of the two parameters (see Brown et al. 1978). The one consistent feature of a TVS is that peak Doppler velocities toward and away from the radar are approximately one beamwidth apart.

A strong TVS is simulated at the center of the core region of the parent mesocyclone in Fig. 4.9.1; a tornado is not simulated because the simulated radar beam has zero width and therefore a tornado would not be properly degraded into a TVS. A comparison of the pattern in Fig. 4.9.1 with the one in Fig. 4.3.2 for a mesocyclone by itself shows that higher velocities extend toward the center of the mesocyclone owing to the presence of the TVS. Figure 4.9.2 illustrates the situation where the TVS is slightly to the right of the mesocyclone center. Again, the TVS makes its presence known because significant velocities extend across the center of the mesocyclone signature where one would expect Doppler velocities to otherwise approach zero when the center of the radar beam coincides with the mesocyclone center. When a strong TVS is located away from the mesocyclone center (Fig. 4.9.3), it takes on a signature more of its own, but each circulation signature is affected by the presence of the other.

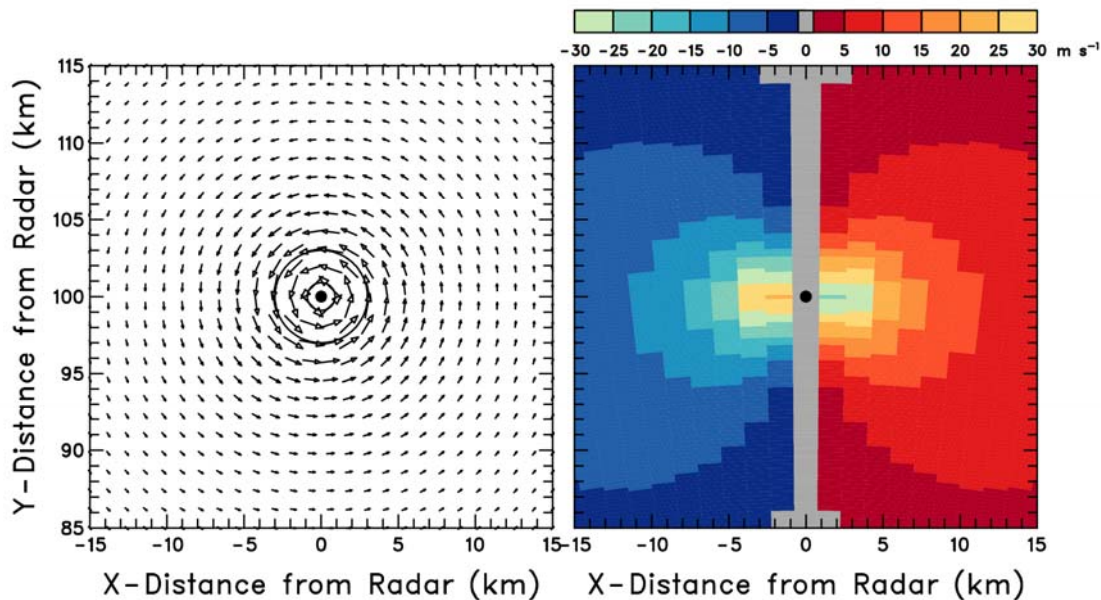


**Fig. 4.9.1.** Doppler velocity pattern (right) corresponding to a TVS (not the tornado itself; peak TVS velocity is  $40 \text{ m s}^{-1}$  or  $78 \text{ kt}$ , core radius is  $0.9 \text{ km}$  or  $0.5 \text{ n mi}$ ) located at the mesocyclone center (peak velocity is  $25 \text{ m s}^{-1}$  or  $49 \text{ kt}$ , core radius is  $3 \text{ km}$  or  $1.6 \text{ n mi}$ ). Black dot represents the coincident mesocyclone and TVS centers. The mesocyclone's core region is within the circle (left panel). Aliased velocities occur at the TVS location (right panel).

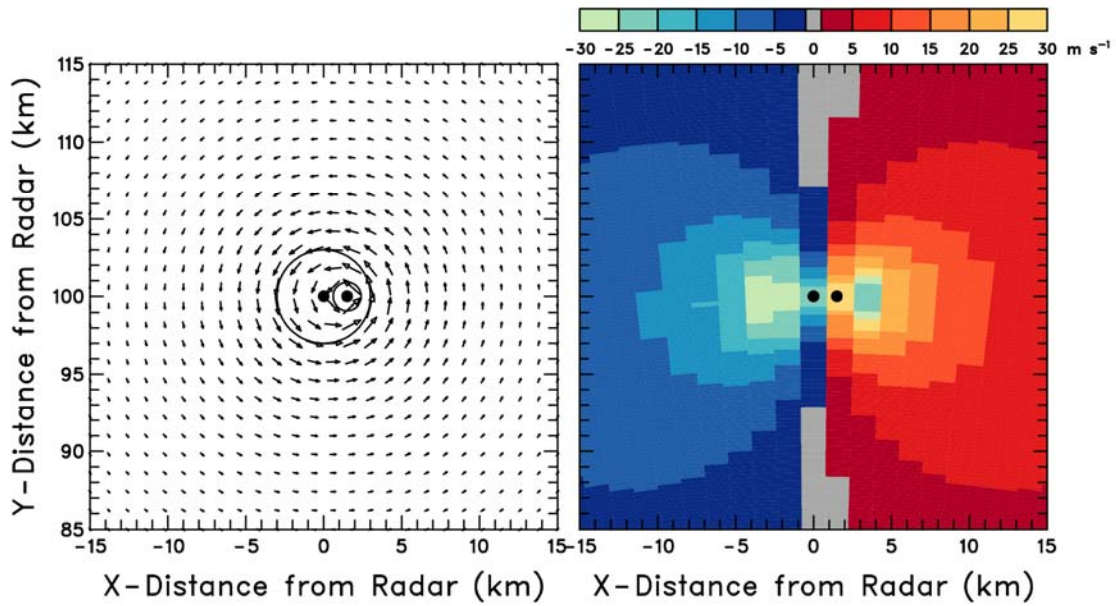


**Fig. 4.9.2.** Same as Fig. 4.9.1, except that the TVS center is located 1.5 km east of the mesocyclone center. The larger and smaller circles in the left panel represent the extent of the mesocyclone and TVS core regions, respectively.

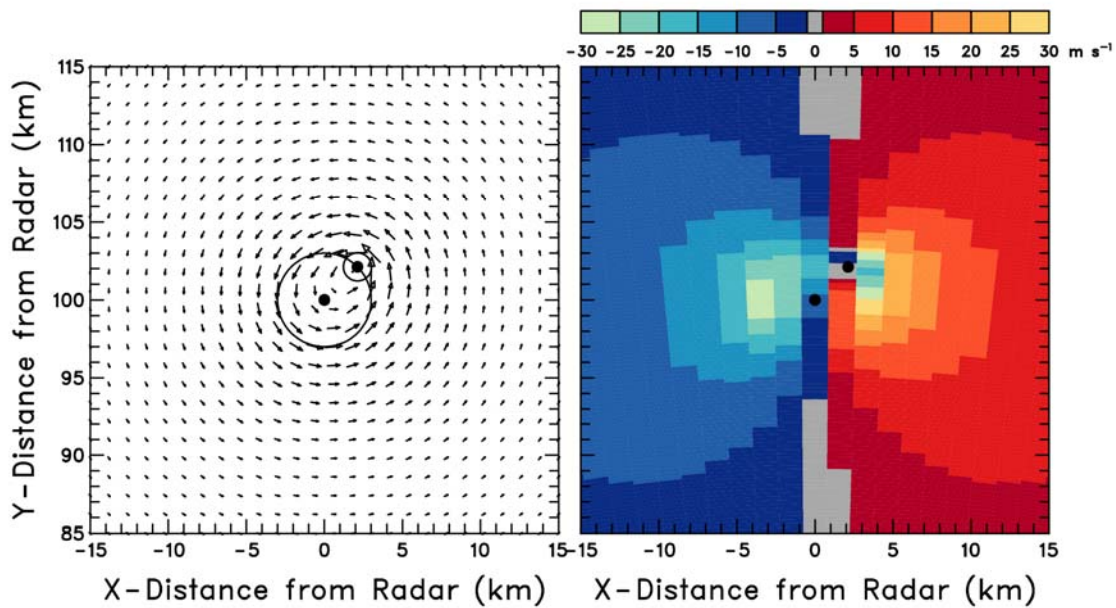


**Fig. 4.9.3.** Same as Fig. 4.9.2, except that the TVS center is located at the edge of the core region 3.0 km northeast of the mesocyclone center.

#### 4.10 Patterns Associated with Two Divergence Regions

Air diverging out from a point source is observed in the atmosphere near storm top in the upper portions of an updraft and near the earth's surface beneath a downdraft (a microburst). When two updrafts or downdrafts are near each other, the corresponding divergent flow fields interact with each other.

Shown in Fig. 4.10.1 are two identical divergence regions, whose centers are separated by three core radii. The individual divergence patterns are not symmetric owing to interaction of the flow fields. The positive Doppler velocity portion of the southwestern divergence region strengthens the positive portion and weakens the negative portion of the northeastern divergence region. Analogously, the negative Doppler velocity portion of the northeastern divergence region strengthens the negative portion and weakens the positive portion of the southwestern divergence region. Note the presence of aliased Doppler velocity values where the flow in one divergence region was enhanced by flow in the other. The region of apparent clockwise rotation at the center of the window actually represents deformation as shown in the left panel.

The Doppler velocity pattern in Fig. 4.10.2 reflects the proximity of two unequal divergence regions with the larger and stronger one located southwest of the smaller and weaker one. Though the larger and stronger divergence region dominates, the interaction of the flow fields still produces a mutual modification of the Doppler velocity patterns for the two outflow regions.

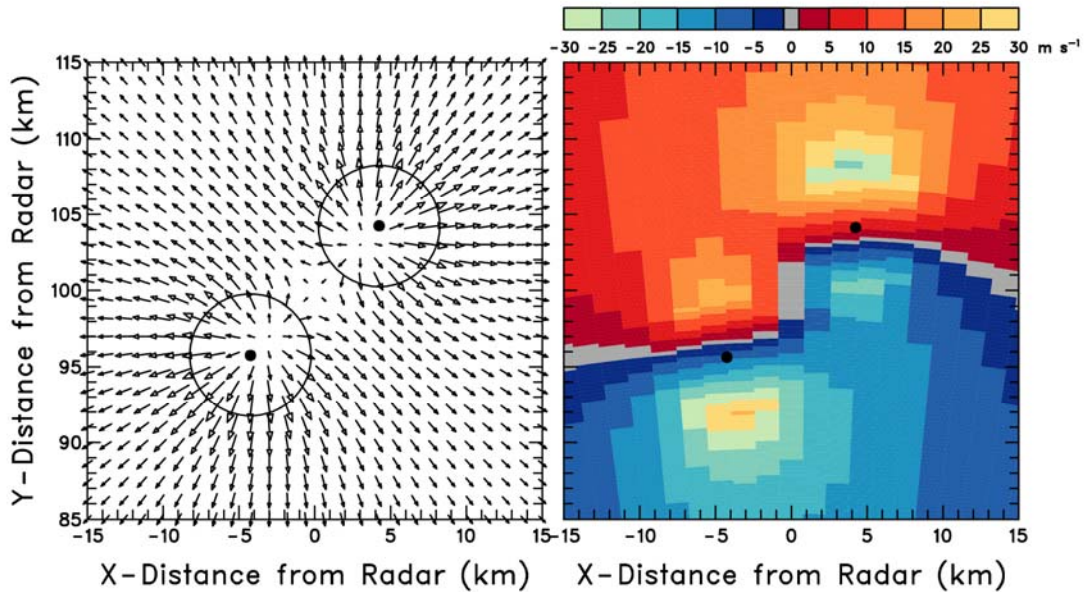


**Fig. 4.10.1.** Doppler velocity pattern (right) corresponding to two divergence regions having the same size (core radius of 4 km or 2.2 n mi) and strength ( $30 \text{ m s}^{-1}$  or 58 kt). The centers of the two divergence centers are 12 km (6.5 n mi) apart and are oriented at a  $45^\circ$  angle to the radar viewing direction. Black dots represent divergence centers. Arrow length is proportional to wind speed. Negative (positive) Doppler velocities represent flow toward (away from) the radar.

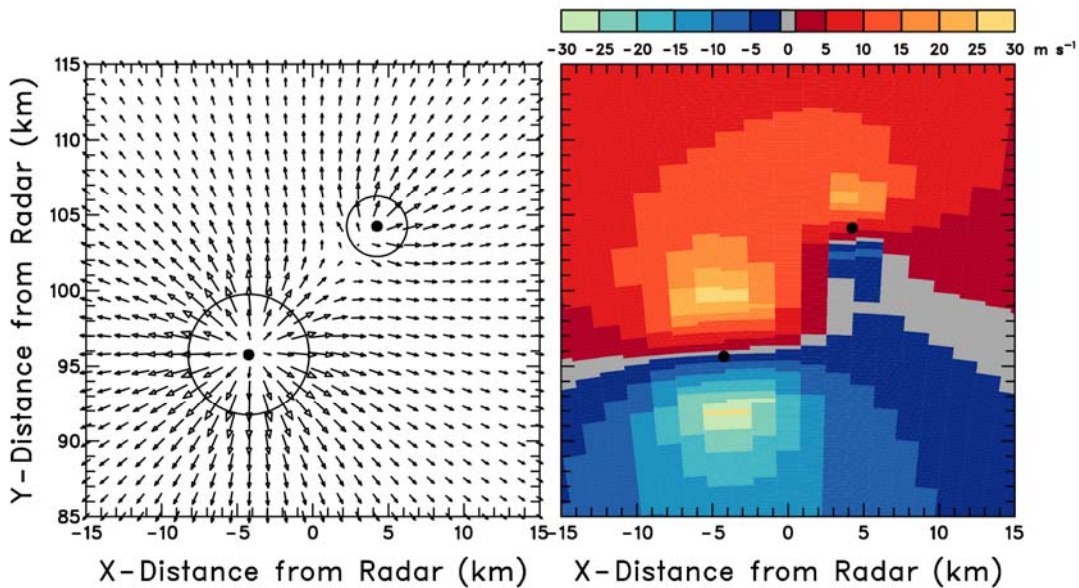


**Fig. 4.10.2.** Same as Fig. 4.10.1, except that the divergence center to the northeast is weaker and smaller with a peak radial velocity of  $15 \text{ m s}^{-1}$  (29 kt) and a core radius of 2 km (1.1 n mi).

#### 4.11 Patterns Associated with Flow Fields beneath Supercell Thunderstorms

Two dominant surface features of a mature supercell thunderstorm are (a) overall cyclonic flow around the storm's rotating updraft (mesocyclone) and (b) the gust front at the leading edge of the cold air expanding outward from the rear flank downdraft. These features are simulated in the left portions of Figs. 4.11.1–4.11.3. A third (secondary) feature is included in the simulation to represent the frequently-observed increase in speed of air converging into the updraft ahead of the gust front.

The simulated flow fields and associated Doppler velocity displays in Figs. 4.11.1–4.11.3 represent storms nominally moving toward the northeast, east, and southeast, respectively, when viewed by a Doppler radar located 50 km due south of the circulation center. The overall Doppler velocity pattern for a storm moving toward the northeast (Fig. 4.11.1) resembles that for a mesocyclone. The pattern is modified by strong flow away from the radar ahead of the gust front. The small negative area south of the mesocyclone center is due to a small region of diffluent air behind the southern end of the gust front that has a component toward the radar.

With the storm moving toward the east, the overall flow pattern is rotated by  $45^\circ$  (Fig. 4.11.2). The increased component of flow toward the radar immediately behind the gust front results in a secondary peak in the negative Doppler velocity values. The strong winds ahead of the front enhance the positive Doppler velocity portion of the mesocyclone signature.

When the pattern is rotated an additional  $45^\circ$  (Fig. 4.11.3), representing storm motion toward the southeast, strong winds ahead of and behind the gust front form a misshapen mesocyclone signature. Flow behind the front enhances the negative Doppler velocity portion of the mesocyclone signature.

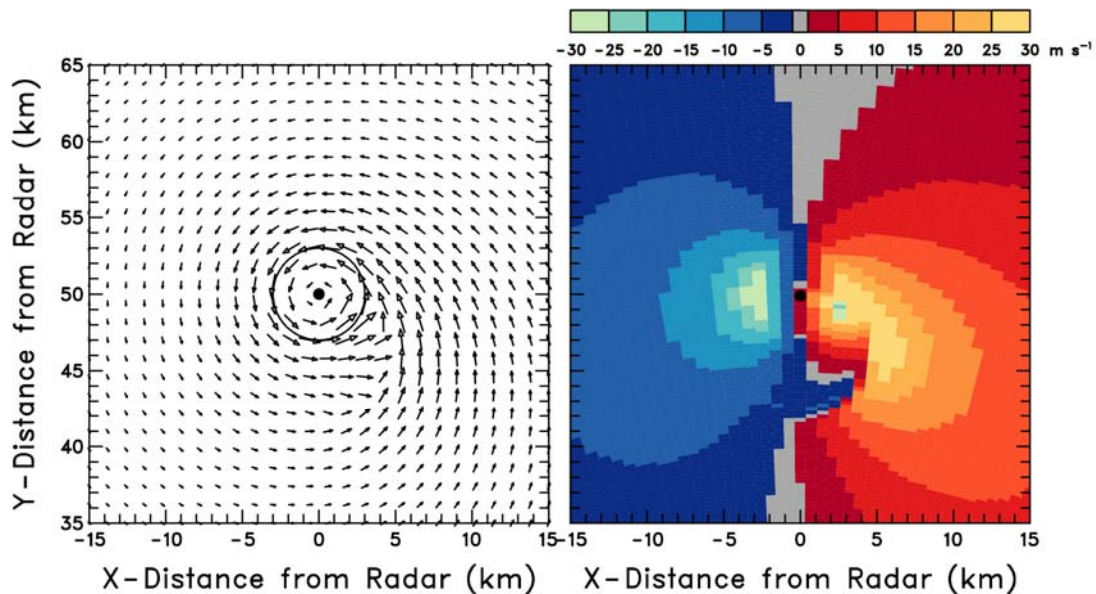


**Fig. 4.11.1.** Doppler velocity pattern (right) corresponding to cyclonic surface flow into the supercell's updraft with enhanced inflow ahead of the gust front (left). The storm is assumed to be moving toward the northeast. Note aliasing of the peak positive Doppler velocity values.

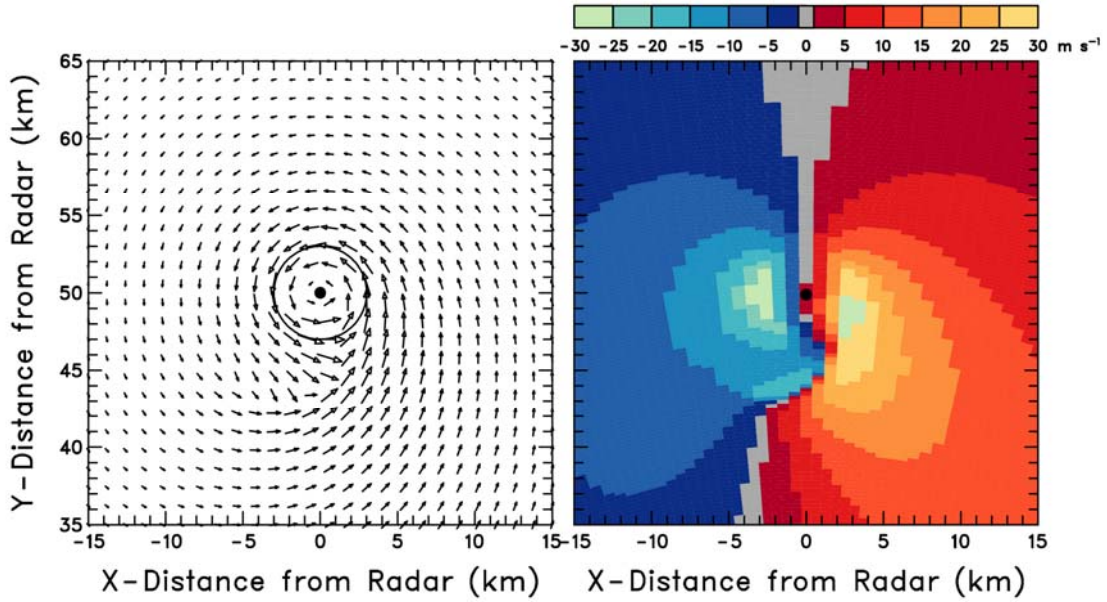


*Fig. 4.11.2. Same as Fig. 4.11.1, except that the storm is assumed to be moving toward the east.*

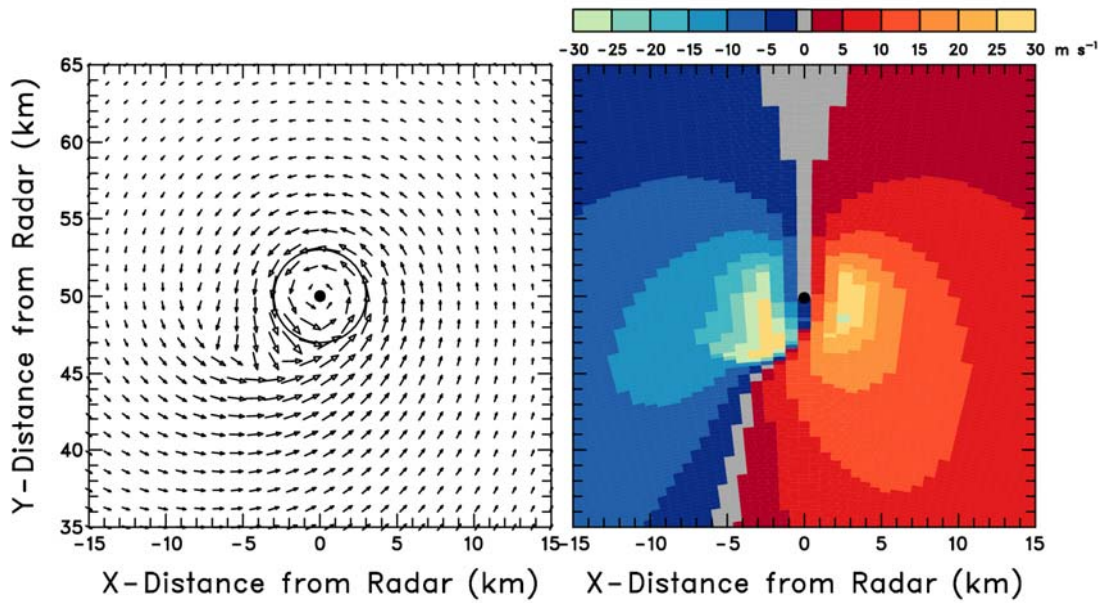


*Fig. 4.11.3. Same as Fig. 4.11.1, except that the storm is assumed to be moving toward the southeast. Note slight aliasing of both the peak positive and negative Doppler velocity values.*

#### 4.12 Patterns Associated with Midaltitude Flow around a Thunderstorm Updraft Region

The updraft region in the upwind portion of a thunderstorm typically interacts with midaltitude flow that overtakes the slower-moving storm (e.g., Brown 1989; Brown and Torgerson 2005). Evidently, the vertical momentum of the strong individual updrafts and pressure perturbations associated with the updraft region present enough resistance to the approaching flow that air slows down as it passes through the semiporous updraft region. As air farther upstream approaches the area of slower-moving air with its higher perturbation pressure, some of the air is diverted around the updraft region. The diverted air increases speed as it is forced to flow around the edges of the updraft region. A developing area of wake flow—that forms directly downstream of the updraft region—includes a narrow swath of low-speed air. The center of the wake contains a train of speed minima. Each minimum forms at the downstream edge of the dominant updraft within the updraft region where some of the diverted air converges from both sides into a localized low-pressure region and descends as a weak downdraft. When the updraft dies, the minimum moves downstream with air continuing to converge into it. Successive dominant updrafts produce the train of successive minima that eventually flow out the downstream end of the storm.

This midaltitude flow pattern is simulated in the left portions of Figs. 4.12.1–4.12.4. The circle approximates the updraft region. The dot near the upstream edge of the circle is the center of axisymmetric divergence that simulates diverging flow around the updraft region. The other two dots within the circle represent a vortex pair (cyclonic on right, anticyclonic on left) that is used to produce increased speeds around the updraft region and decreased speeds within the updraft region. The pairs of downstream dots represent successively weaker vortex pairs that are used to simulate the low-speed wake region.

The Doppler velocity pattern in the right portion of Fig. 4.12.1 represents the type of midaltitude pattern that one might expect to see when a Doppler radar scans across a thunderstorm from an upstream location. Doppler velocity maxima occur on the lateral flanks of the overall updraft region and Doppler velocity minima occur through the center of the storm. It is typical for localized minima to occur within the wake and for localized maxima to occur along the flanks of the wake region.

When radar views the midaltitude flow at 30° and 60° angles (Figs. 4.12.2 and 4.12.3, respectively), the pattern of the low-speed wake region is still evident downstream of the updraft region. However, the Doppler velocity maximum on the right flank of the updraft region is greatly reduced because most of the strong flow on that flank is perpendicular to the radar viewing direction. At these viewing angles, the radar is sensing some of the divergent component of flow around the updraft region, which is indicated by the extreme positive and negative Doppler velocity areas on the fringes of the updraft region.

When the viewing direction is perpendicular to the overall flow, the presence of a wake is no longer readily evident (Fig. 4.12.4). Instead, there is a prominent divergence signature associated with air diverging around the updraft region. Farther downstream, the wake region is represented by weak convergence signatures associated with air converging into the localized speed minima.

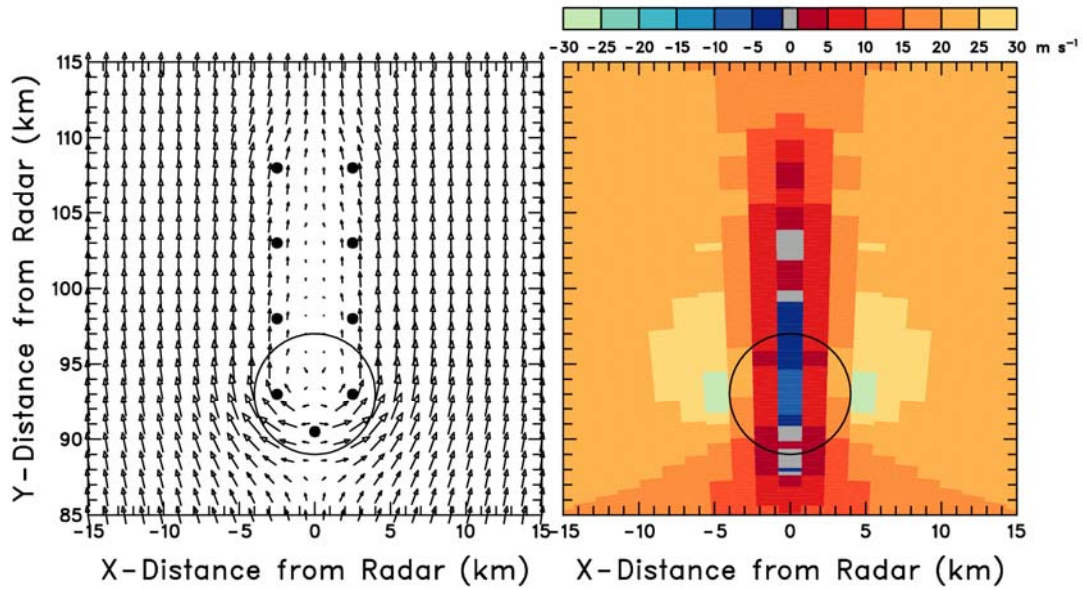


**Fig. 4.12.1.** Doppler velocity pattern (right) corresponding to ground-relative midaltitude flow (left) around a strong thunderstorm updraft region (circle). Arrow length is proportional to wind speed. The radar viewing direction is parallel to the overall environmental wind. See text for an explanation of the dots in the left panel. Note that Doppler velocity aliasing occurs in the strong flow around the circled updraft region.

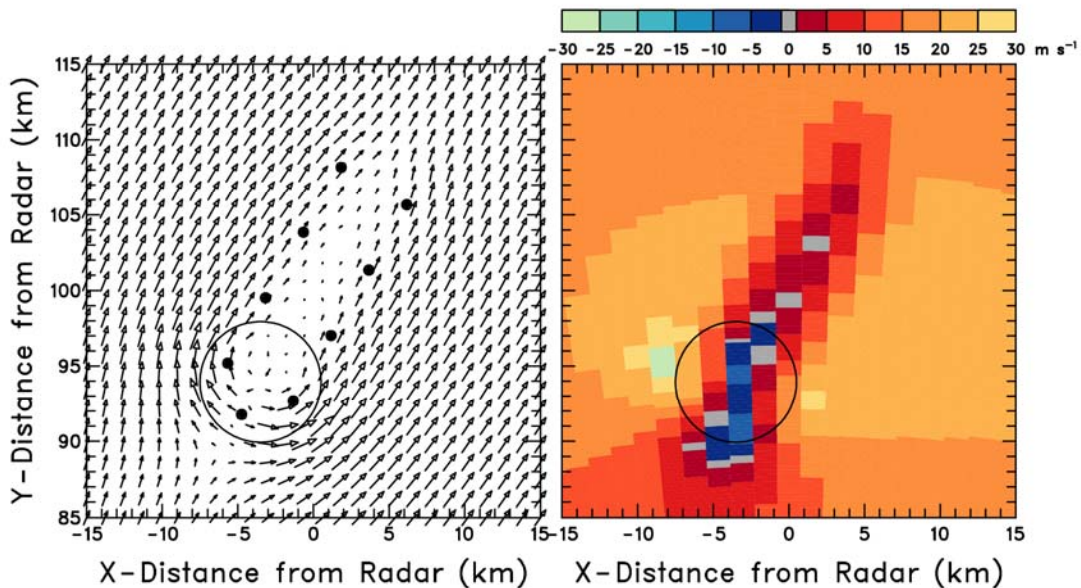


**Fig. 4.12.2.** Same as Fig. 4.12.1, except that the radar viewing direction is at a  $30^\circ$  angle to the overall environmental flow.

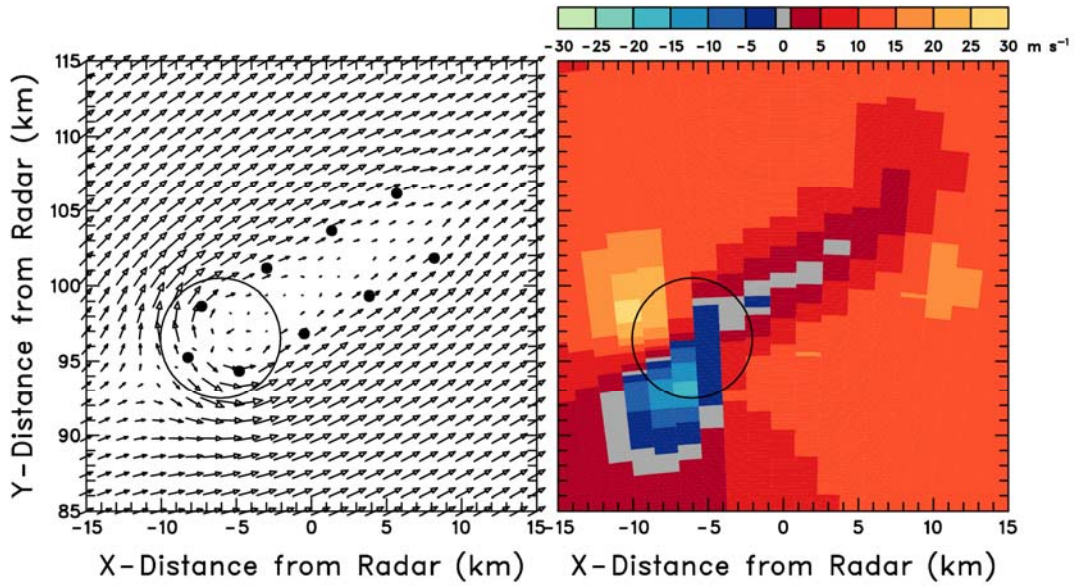


**Fig. 4.12.3.** Same as Fig. 4.12.1, except that the radar viewing direction is at a  $60^\circ$  angle to the overall environmental flow.

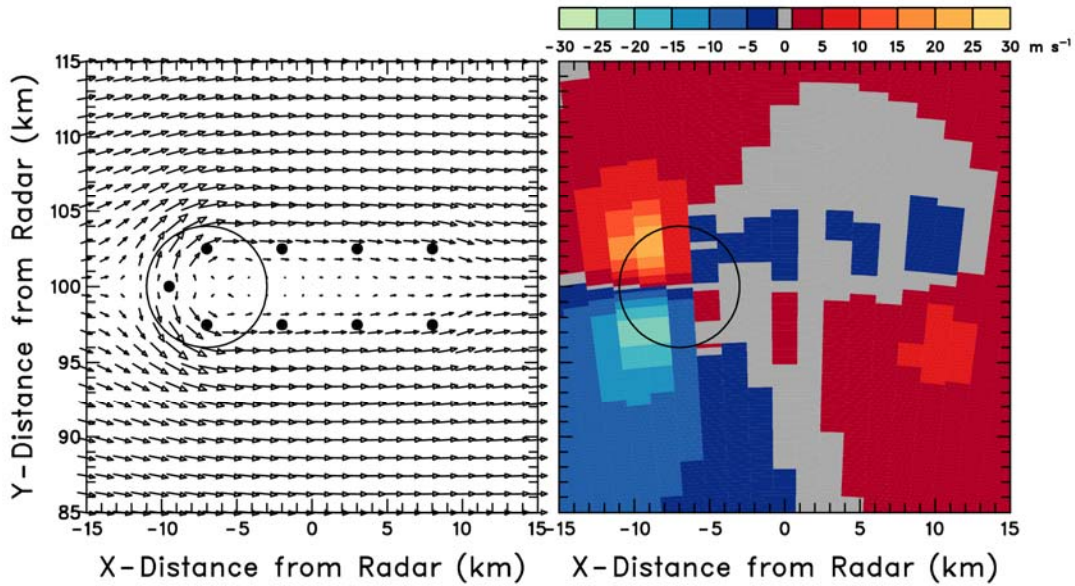


**Fig. 4.12.4.** Same as Fig. 4.12.1, except that the radar viewing direction is perpendicular to the overall environmental flow.

## 5. THE CHALLENGE

The goal of this Guide is to introduce the use of pattern recognition techniques for interpreting single Doppler velocity data. It is hoped that the use of simulated flow fields has helped to bring out the basic features that one may find somewhat masked in actual data.

The initial challenge for the reader is to understand why the Doppler velocity patterns in this Guide appear as they do. One must remember that storms will not always be located to the north of the radar. It also is important to recognize that the presence of Doppler components of storm motion and environmental wind in the data do not affect the overall Doppler velocity *patterns*.

The ultimate challenge, however, is to use the understanding gained from mastering this Guide to interpret the more complicated Doppler velocity patterns found in the real world. Proper interpretation of Doppler velocity patterns should result in a better understanding of atmospheric processes. For the forecaster, proper interpretation of Doppler velocity patterns should manifest itself through the issuance of more timely and accurate warnings and short-term forecasts.

Good Luck!

## 6. ACKNOWLEDGMENTS

### *First Edition of the Guide (1987):*

We appreciate the contributions made by our colleagues at the National Severe Storms Laboratory, the NEXRAD Operational Support Facility, and the National Weather Service Forecast Office in Norman. Don Burgess, who is a long-time supporter and interpreter of single Doppler radar data, assisted us with the planning of this Guide. Recognizing the critical need for training in Doppler velocity interpretation, Ken Wilk has actively supported the Guide's preparation. Tim O'Bannon modified computer programs that made possible the color Doppler velocity displays used here. Joe Kendall provided valuable comments through his position as the Training Activities Meteorologist for the WSFO. Ruth Miller typed the manuscript and Joan Kimpel provided graphic arts support. This Guide was funded through a Memorandum of Understanding between the NEXRAD Joint System Program Office and the National Severe Storms Laboratory.

### *Second Edition of the Guide (2007):*

All of the color figures and associated flow fields in this edition of the Guide were prepared by the second author using NCAR Graphics. The color scales used herein are based on those developed by Cynthia Brewer (Pennsylvania State University) to be color blind friendly (<http://ColorBrewer.org>). Figures 1.2.1, 1.2.2, and 2.1.1 were prepared by Joan O'Bannon. We appreciate the comments and suggestions by Jami Boettcher (National Weather Service's Warning Decision Training Branch), Donald Burgess (Cooperative Institute for Mesoscale Meteorological Studies, University of Oklahoma), Pat Kennedy (Colorado State University), and Jennifer Palucki and John Pike (NWS Forecast Office, Oklahoma City/Norman).

## REFERENCES

- Battan, L. J., 1973: *Radar Observation of the Atmosphere*. Univ. of Chicago Press, Chicago, 324 pp.
- Baynton, H. W., 1979: The case for Doppler radars along our hurricane-affected coasts. *Bull. Amer. Meteor. Soc.*, **60**, 1014–1023.
- \_\_\_\_\_, R. J. Serafin, C. L. Frush, G. R. Gray, P. V. Hobbs, R. A. Houze, Jr., and J. D. Locatelli, 1977: Real-time wind measurement in extratropical cyclones by means of Doppler radar. *J. Appl. Meteor.*, **16**, 1022–1028.
- Brown, R. A., 1989: Initiation and propagation of thunderstorm mesocyclones. Ph.D. dissertation, University of Oklahoma, 321 pp. [Available from University Microfilms, Ann Arbor, MI, No. 89-19983.]
- \_\_\_\_\_, and V. T. Wood, 1991: On the interpretation of single-Doppler velocity patterns within severe thunderstorms. *Wea. Forecasting*, **6**, 32–48.
- \_\_\_\_\_, and K. Torgerson, 2005: Interpretation of single-Doppler radar signatures in a V-shaped hailstorm: Part II – Evolution of updraft interactions with ambient midaltitude flow. *Natl. Wea. Dig.*, **29**, 65–80.
- \_\_\_\_\_, L. R. Lemon, and D. W. Burgess, 1978: Tornado detection by pulsed Doppler radar. *Mon. Wea. Rev.*, **106**, 29–38.
- Burgess, D. W., V. T. Wood, and R. A. Brown, 1982: Mesocyclone evolution statistics. Preprints, *12<sup>th</sup> Conf. on Severe Local Storms*, San Antonio, Amer. Meteor. Soc., 422–424.
- Conway, J. W., K. D. Hondl, M. J. Moreland, J. M. Cordell, and R. J. Harron, 1995: Improvements in the WSR–88D dealiasing algorithm: The pursuit of the final, most important gates. Preprints, *27<sup>th</sup> Conf. on Radar Meteor.*, Vail, CO, Amer. Meteor. Soc., 145–147.
- Doviak, R. J., and D. S. Znić, 1993: *Doppler Radar and Weather Observations*. Second edition, Academic Press, Orlando, 562 pp.
- Eilts, M. D., and S. D. Smith, 1990: Efficient dealiasing of Doppler velocities using local environment constraints. *J. Atmos. Oceanic Technol.*, **7**, 118–128.
- OFC, 2006: Doppler radar meteorological observations, Part C, WSR–88D products and algorithms. Federal Meteorological Handbook 11, FCM-H11C-2006, Office of the Federal Coordinator for Meteorological Services and Supporting Research, Silver Spring, MD. Available online at: <http://www.ofcm.gov/fmh11/fmh11.htm>.
- Kraus, M. J., and R. J. Donaldson, Jr., 1976: Interpretation of PPI velocity displays in widespread storms. Preprints, *17<sup>th</sup> Conf. on Radar Meteor.*, Seattle, Amer. Meteor. Soc., 239–243.
- Rinehart, R. E., 2004: *Radar for Meteorologists*. Fourth ed., Rinehart Publications, Columbia, MO, 482 pp.
- Rogers, R. R., 1990: The early years of Doppler radar in meteorology. Chapter 16 in *Radar in Meteorology*, D. Atlas, Ed., Amer. Meteor. Soc., Boston, 122–129.
- Wood, V. T., and R. A. Brown, 1986: Single Doppler velocity signature interpretation of nondivergent environmental winds. *J. Atmos. Oceanic Technol.*, **3**, 114–128.
- \_\_\_\_\_, and \_\_\_\_\_, 1992: Effects of radar proximity on single-Doppler velocity signatures of axisymmetric rotation and divergence. *Mon. Wea. Rev.*, **120**, 2798–2807.
- \_\_\_\_\_, and \_\_\_\_\_, 1997: Effects of radar sampling on single-Doppler velocity signatures of mesocyclones and tornadoes. *Wea. Forecasting*, **12**, 928–938.